

# A six-dimensional $\text{H}_2\text{-H}_2$ potential energy surface for bound state spectroscopy

Robert J. Hinde\*

*Department of Chemistry, University of Tennessee, Knoxville, Tennessee 37996-1600*

We present a six-dimensional potential energy surface for the  $(\text{H}_2)_2$  dimer based on coupled-cluster electronic structure calculations employing large atom-centered Gaussian basis sets and a small set of midbond functions at the dimer's center of mass. The surface is intended to describe accurately the bound and quasibound states of the dimers  $(\text{H}_2)_2$ ,  $(\text{D}_2)_2$ , and  $\text{H}_2\text{-D}_2$  that correlate with  $\text{H}_2$  or  $\text{D}_2$  monomers in the rovibrational levels  $(v, j) = (0, 0)$ ,  $(0, 2)$ ,  $(1, 0)$ , and  $(1, 2)$ . We employ a close-coupled approach to compute the energies of these bound and quasibound dimer states using our potential energy surface, and compare the computed energies for infrared and Raman transitions involving these states with experimentally measured transition energies. We use four of the experimentally measured dimer transition energies to make two empirical adjustments to the ab initio potential energy surface; the adjusted surface gives computed transition energies for 56 experimentally observed transitions that agree with experiment to within  $0.036 \text{ cm}^{-1}$ . For 29 of the 56 transitions, the agreement between the computed and measured transition energies is within the quoted experimental uncertainty. Finally, we use our potential energy surface to predict the energies of another 34 not-yet-observed infrared and Raman transitions for the three dimers.

Submitted to J. Chem. Phys. 22 Aug 2007; accepted 27 Nov 2007

PACS numbers: 34.20.Cf, 31.25.-v, 36.40.-c

## I. INTRODUCTION

The  $(\text{H}_2)_2$  dimer has long been viewed as a prototypical bimolecular van der Waals dimer. Because the  $(\text{H}_2)_2$  dimer is electronically simple, it has been the focus of a number of ab

initio studies,<sup>1,2,3,4,5,6,7,8,9,10,11,12,13,14,15,16,17</sup> however, because the H<sub>2</sub>–H<sub>2</sub> van der Waals interaction is quite weak,<sup>18</sup> ab initio calculations with accuracy much higher than the oft-quoted “chemical accuracy” of 1 kcal/mol must be employed to provide useful information about the H<sub>2</sub>–H<sub>2</sub> potential energy surface. Two recent advances in ab initio methods have made it possible to compute the H<sub>2</sub>–H<sub>2</sub> interaction with the required level of accuracy: (1) the development of hierarchical sequences of one-electron Gaussian basis sets for approximating molecular electronic wave functions,<sup>19</sup> sequences which systematically approach the complete one-electron basis set limit, and (2) the development of efficient methods for accounting for electron correlation effects in these wave functions by systematically approaching the many-electron basis set limit.<sup>20,21</sup>

Diep and Johnson<sup>14,15</sup> took advantage of these two advances in ab initio methods to compute an accurate four-dimensional rigid rotor potential energy surface for the (H<sub>2</sub>)<sub>2</sub> dimer; the Diep–Johnson surface gives low temperature second virial coefficients and integral elastic scattering cross sections in reasonably good agreement with experiment. However, this potential energy surface does not depend explicitly on the covalent bond lengths of the two H<sub>2</sub> monomers, and thus is only able to describe the interaction between two H<sub>2</sub> molecules in their  $v = 0$  vibrational ground states.

More recently, Boothroyd *et al.*<sup>17</sup> have compiled a large database of energies for the H<sub>4</sub> system, based largely on multireference configuration interaction ab initio calculations, and have fit a global six-dimensional H<sub>4</sub> potential energy surface to these energies. However, in this database, (H<sub>2</sub>)<sub>2</sub> dimer configurations representative of the van der Waals well are assigned energies that come not from ab initio calculations, but rather from an empirically modified rigid rotor potential energy surface. Recent theoretical studies of low-energy inelastic H<sub>2</sub>–H<sub>2</sub> collisions that use this potential energy surface<sup>22,23,24</sup> yield computed energy transfer rate coefficients in rather poor agreement with experiment.

The (H<sub>2</sub>)<sub>2</sub> dimer has also been the focus of several experimental investigations, beginning with the pioneering work of Watanabe and Welsh<sup>25</sup> that demonstrated the dimer’s existence through observation of its infrared (IR) absorption spectrum in the H<sub>2</sub>  $v = 1 \leftarrow 0$  vibrational fundamental band. Later experimental studies<sup>26,27</sup> recorded at high resolution the IR absorption spectra of the (H<sub>2</sub>)<sub>2</sub> dimer (and several of its isotopomers) in the  $v = 1 \leftarrow 0$  fundamental band and  $v = 2 \leftarrow 0$  first overtone band of the corresponding monomers. The high resolution IR absorption spectra of (H<sub>2</sub>)<sub>2</sub> in the H<sub>2</sub> fundamental and overtone regions, and

the analogous isotopomer spectra, provide information about the vibrational dependence of the  $\text{H}_2\text{-H}_2$  interaction. Complementary studies<sup>28</sup> of the far-IR absorption spectrum of the dimer provide information about the anisotropy of the potential energy surface in the region of the van der Waals well.

Recently, the Raman spectrum of the  $(\text{H}_2)_2$  dimer in the  $\text{H}_2$  fundamental region has also been observed.<sup>29</sup> This spectrum provides information about the vibrational dependence of the  $\text{H}_2\text{-H}_2$  interaction that is complementary to that provided by the high-resolution IR studies. Specifically, the vibrationally excited state of  $(\text{H}_2)_2$  that is probed by the IR studies is one in which the vibrational excitation is delocalized across the two  $\text{H}_2$  monomers in an antisymmetric fashion, while in the Raman studies, the excited  $(\text{H}_2)_2$  state is one in which the vibrational excitation is delocalized symmetrically across the two monomers. A comparison of the IR and Raman spectra thus provides insight into the coupling between the two  $\text{H}_2$  vibrational modes in the  $(\text{H}_2)_2$  complex and into the dependence of the  $\text{H}_2\text{-H}_2$  potential energy surface on the two monomers' bond lengths.

Equipped with this new information, we attempt here the construction of a six-dimensional  $\text{H}_2\text{-H}_2$  potential energy surface that accurately describes the dimer's van der Waals well. We begin by computing ab initio  $\text{H}_2\text{-H}_2$  interaction energies that are nearly converged with respect to both the one-electron and many-electron basis sets, and then construct a smooth potential energy surface from these computed interaction energies. We then make two small empirical adjustments to the surface; these adjustments soften slightly the surface's short-range repulsive wall, and increase slightly the strength of the surface's anisotropic term that couples the rotational degrees of freedom of the two monomers. The empirically adjusted surface gives IR and Raman transition energies for the (*para*- $\text{H}_2$ )<sub>2</sub>, (*ortho*- $\text{D}_2$ )<sub>2</sub>, and *para*- $\text{H}_2$ -*ortho*- $\text{D}_2$  dimers in good agreement with available experimental data.<sup>26,28,29</sup>

## II. AB INITIO COMPUTATIONS

### A. Functional form of the $\text{H}_2\text{-H}_2$ interaction

We consider a space-fixed coordinate system  $(x, y, z)$  in which one  $\text{H}_2$  molecule (denoted molecule 1) has its center of mass at the origin and the other  $\text{H}_2$  molecule (denoted molecule

2) has its center of mass on the positive  $z$  axis. The orientation of molecule  $i$  is specified by its spherical polar and azimuthal angles  $(\theta_i, \phi_i)$ . We let  $R$  represent the distance between the molecules' centers of mass, and let  $r_i$  represent the bond length of molecule  $i$ . The H<sub>2</sub>–H<sub>2</sub> potential energy surface can then be expanded in terms of coupled spherical harmonics:<sup>30</sup>

$$V = \sum_{l_1, l_2, L} A_{l_1, l_2, L}(R, r_1, r_2) G_{l_1, l_2, L}(\theta_1, \theta_2, \phi) \quad (1)$$

where  $\phi = \phi_2 - \phi_1$ , the summation indices  $l_1$ ,  $l_2$ , and  $L$  are non-negative integers that must satisfy

$$l_1 + l_2 + L = \text{even integer}, \quad (2)$$

and the homonuclear symmetry of the two H<sub>2</sub> monomers dictates that  $l_1$  and  $l_2$  are also both even. The angular functions  $G_{l_1, l_2, L}$  have the form

$$G_{l_1, l_2, L} = \sqrt{\frac{2L+1}{4\pi}} \sum_m C(l_1, m, l_2, -m; L, 0) Y_{l_1, m}(\theta_1, \phi_1) Y_{l_2, -m}(\theta_1, \phi_2) \quad (3)$$

where  $C$  is a Clebsch–Gordan coefficient and  $Y_{l, m}$  is a spherical harmonic normalized so that  $Y_{l, m}(0, 0) = \delta_{m, 0} \sqrt{(2l+1)/4\pi}$ . (We use the Condon–Shortley phase convention for  $Y_{l, m}$ .) The appearance of the Clebsch–Gordan coefficient  $C$  in Eq. (3) means that  $l_1$ ,  $l_2$ , and  $L$  must satisfy the angular momentum triangle rule.

The functions  $G_{l_1, l_2, L}$  constitute a complete, orthogonal basis set for functions of the three angular coordinates  $(\theta_1, \theta_2, \phi)$ . For fixed  $R$ ,  $r_1$ , and  $r_2$ , the coefficient  $A_{l_1, l_2, L}(R, r_1, r_2)$  can therefore be computed as

$$A_{l_1, l_2, L}(R, r_1, r_2) = \frac{1}{2L+1} \int \int G_{l_1, l_2, L}(\theta_1, \theta_2, \phi) V(R, r_1, r_2, \theta_1, \theta_2, \phi) dS_1 dS_2 \quad (4)$$

where  $dS_i = \sin \theta_i d\theta_i d\phi_i$ .

Earlier studies of the four-dimensional rigid-rotor H<sub>2</sub>–H<sub>2</sub> potential energy surface<sup>14,15,18</sup> show that the surface is dominated by four terms, with  $(l_1, l_2, L) = (0, 0, 0)$ ,  $(0, 2, 2)$ ,  $(2, 0, 2)$ , and  $(2, 2, 4)$ . In this work, we use numerical quadrature to compute the right-hand side of Eq. (4) for these four  $(l_1, l_2, L)$  triples. Specifically, at fixed values of  $R$ ,  $r_1$ , and  $r_2$ , we use the 18-point spherical quadrature rule numbered 25.4.64 in Ref. 31 to evaluate the integrals over both  $dS_1$  and  $dS_2$  in Eq. (4). This requires us to compute the H<sub>2</sub>–H<sub>2</sub> interaction energy  $V(R, r_1, r_2, \theta_1, \theta_2, \phi)$ , using ab initio quantum chemical methods that we describe in the next subsection, at 12 sets of angles  $(\theta_1, \theta_2, \phi)$  when  $r_1 = r_2$  and at 19 sets of angles when

$r_1 \neq r_2$ . Symmetry relationships allow the rest of the  $18^2 = 324$  interaction energies at fixed  $(R, r_1, r_2)$  to be determined from these ab initio calculations.

The accuracy of the  $A_{l_1, l_2, L}$  coefficients computed in this fashion is limited by the fact that the quadrature rule we use fails to reproduce the orthogonality conditions

$$\int \int G_{l_1, l_2, L}(\theta_1, \theta_2, \phi) G_{l'_1, l'_2, L'}(\theta_1, \theta_2, \phi) dS_1 dS_2 = \delta_{l_1, l'_1} \delta_{l_2, l'_2} \delta_{L, L'} (2L + 1) \quad (5)$$

when  $l_1 + l'_1 \geq 6$  or  $l_2 + l'_2 \geq 6$ . This means that the value of  $A_{0,0,0}$  obtained via quadrature also includes some contamination from  $A_{6,0,6}$  and  $A_{0,6,6}$  (if these coefficients are nonzero in the ab initio potential energy surface), while  $A_{2,2,4}$  is contaminated by (among other terms)  $A_{2,4,6}$  and  $A_{4,2,6}$ , which describe the long-range electrostatic quadrupole–hexadecapole (QH) interaction between the two  $\text{H}_2$  molecules.

To assess the magnitude of these erroneous contributions to the four  $A_{l_1, l_2, L}$  coefficients of interest, we used the more accurate 24-point spherical quadrature rule of Ref. 31 to calculate the coefficients at  $(R, r_1, r_2) = (4.5 a_0, 1.4 a_0, 1.7 a_0)$ , a repulsive  $(\text{H}_2)_2$  configuration where we expect the angular anisotropy of the potential energy surface to be relatively high, and where this contamination should thus be relatively severe. Table I compares the coefficients obtained using the two quadrature rules (based on ab initio interaction energies computed using the protocol outlined in Sec. II B); the errors introduced at this  $(R, r_1, r_2)$  configuration by using 18-point quadrature appear to be quite small for the four terms that we include in our final potential energy surface. This table also gives the values for two additional coefficients in the coupled spherical harmonic expansion,  $A_{2,2,0}$  and  $A_{2,2,2}$ , at this  $(\text{H}_2)_2$  configuration, and shows that they are one to two orders of magnitude smaller than any of the four terms we retain in Eq. (1). This is in accord with previous studies<sup>14,15,18</sup> of the four-dimensional rigid-rotor  $\text{H}_2$ – $\text{H}_2$  potential energy surface.

## B. CCSD(T) ab initio calculations

We use Gaussian 03<sup>32</sup> to compute the  $\text{H}_2$ – $\text{H}_2$  interaction energy, employing a coupled-cluster<sup>20,21</sup> treatment of electron correlation that includes single and double excitations and a perturbative treatment of triple excitations,<sup>33</sup> abbreviated CCSD(T). The CCSD(T) calculations are based on a restricted Hartree–Fock reference wave function; we have verified that such a reference does not exhibit a restricted  $\rightarrow$  unrestricted instability for the  $\text{H}_2$  bond

lengths considered here. We use the aug-cc-pVQZ basis set<sup>19,34</sup> for the four hydrogen atoms, supplement this atom-centered basis set with a set of (3s3p2d) bond functions positioned at the dimer’s center of mass, and employ the standard counterpoise correction.<sup>35</sup> The bond function exponents are taken from Ref. 36.

We carry out these calculations at  $r_1$  and  $r_2$  values of 1.1, 1.4, and 1.7  $a_0$ , and at 19  $R$  values ranging from  $R = 4.25 a_0$  to 12.0  $a_0$ , for a total of 1653 unique  $(R, r_1, r_2, \theta_1, \theta_2, \phi)$   $(\text{H}_2)_2$  configurations. We turn off automatic checking of the one-electron overlap matrix for near linear dependence and retain all 206 one-electron basis functions at every configuration; this eliminates possible discontinuities in the potential energy surface that could arise when some of these functions are dropped from the one-electron basis set. The Gaussian 03  $\text{H}_2\text{--H}_2$  total CCSD(T) energies for these configurations are available from the EPAPS depository.<sup>37</sup> We have checked a small subset of these energies against calculations using the Dalton ab initio code;<sup>38</sup> the dimer total energies computed using the two codes agree to within  $2 \times 10^{-8}$  hartrees or better.

To assess the error introduced by truncating the one-electron basis set at the aug-cc-pVQZ + (3s3p2d) level, we performed some calculations at selected configurations using a smaller aug-cc-pVTZ atom-centered basis set and the same (3s3p2d) bond function set. The coefficients  $A_{l_1, l_2, L}$  obtained from these two sets of ab initio interaction energies are listed in Table II. The two sets of coefficients generally differ by no more than 1% to 2%, suggesting that the aug-cc-pVQZ + (3s3p2d) basis set is nearly saturated. Truncating the one-electron basis set seems to have the largest effect on the isotropic coefficient  $A_{0,0,0}$  computed at small values of  $R$ , where the potential energy surface is strongly repulsive.

### C. CCSDT ab initio calculations

Our earlier study of the vibrational dependence of the  $\text{H}_2\text{--H}_2$  interaction<sup>39</sup> indicates that incompleteness in the many-electron basis set could materially affect the shape of the potential energy surface in the van der Waals well. Similar effects have been observed in other weakly-bound dimers of two-valence-electron systems.<sup>40,41</sup> To reduce the error associated with truncation of the many-electron basis set at the CCSD(T) level of theory, we employ a coupled-cluster treatment that includes a fully iterative treatment of single, double, and triple excitations,<sup>42,43</sup> abbreviated CCSDT, to compute the  $\text{H}_2\text{--H}_2$  interaction energy at

selected high-symmetry geometries (those in which  $\theta_1$ ,  $\theta_2$ , and  $\phi$  take values of 0 or  $\pi/2$ ). These calculations are performed using the tensor contraction engine<sup>44</sup> incorporated into version 4.7 of the electronic structure code NWChem.<sup>45,46</sup>

Unfortunately, the CCSDT calculations are prohibitively expensive if we employ the aug-cc-pVQZ + (3s3p2d) one-electron basis set used in the CCSD(T) calculations. We therefore perform the CCSDT calculations using a smaller one-electron basis set consisting of only atom-centered aug-cc-pVTZ functions. We also use NWChem to perform CCSD(T) calculations at these high-symmetry geometries using the atom-centered aug-cc-pVTZ basis set. We then take the difference between the CCSDT and CCSD(T) counterpoise-corrected interaction energies as an additive correction to the aug-cc-pVQZ + (3s3p2d) CCSD(T) potential energy surface. For the sake of brevity, we will call this the “full-triples” correction. We found that to insure convergence of the CCSDT iterations at some geometries, it was necessary to increase the cutoff for computational linear dependence in the one-electron basis set to  $10^{-6}$ . For consistency, we therefore used this cutoff in all of the CCSDT and CCSD(T) calculations performed with NWChem.

Because we compute the full-triples correction at a small number of  $\text{H}_2\text{-H}_2$  orientations  $(\theta_1, \theta_2, \phi)$ , we cannot use the quadrature scheme described in the previous subsection to extract corresponding full-triples corrections to the  $A_{l_1, l_2, L}$  coefficients computed at the CCSD(T) aug-cc-pVQZ + (3s3p2d) level of theory. Instead, we use least-squares techniques to fit the full-triples correction to the function

$$\begin{aligned} &\Delta A_{0,0,0}(R, r_1, r_2)G_{0,0,0}(\theta_1, \theta_2, \phi) + \Delta A_{0,2,2}(R, r_1, r_2)G_{0,2,2}(\theta_1, \theta_2, \phi) \\ &+ \Delta A_{2,0,2}(R, r_1, r_2)G_{2,0,2}(\theta_1, \theta_2, \phi) + \Delta A_{2,2,4}(R, r_1, r_2)G_{2,2,4}(\theta_1, \theta_2, \phi) . \end{aligned} \quad (6)$$

We then add the corrections  $\Delta A_{l_1, l_2, L}$  to the corresponding coefficients  $A_{l_1, l_2, L}$  obtained from four-dimensional quadrature over the CCSD(T) aug-cc-pVQZ + (3s3p2d) interaction energies. The CCSDT and CCSD(T) energies used to compute the full-triples correction are available through EPAPS.<sup>37</sup> For the sake of brevity, we henceforth use the term “coefficients” to mean the sum of the CCSD(T) coefficients and the full-triples corrections.

### D. Construction of a smooth potential energy surface

We now construct a smooth potential energy surface from the ab initio coefficients  $A_{l_1, l_2, L}(R, r_1, r_2)$ . For each pair of  $\text{H}_2$  bond lengths  $(r_1, r_2)$ , we create four cubic splines, one for each of the coefficients  $A_{l_1, l_2, L}$ , that interpolate the 19 coefficient values between  $R = 4.25 a_0$  and  $R = 12.0 a_0$ . We extrapolate the splines to  $R$  values below  $4.25 a_0$  and above  $12.0 a_0$  using functions described in the next two paragraphs. At  $R = 4.25 a_0$ , the slope of each cubic spline is constrained to match the slope of the corresponding small- $R$  extrapolating function.

We extend each cubic spline to  $R$  values below  $4.25 a_0$  using a simple two-parameter exponential extrapolation of the form  $U \exp(-cR)$  that fits the coefficients obtained at  $R = 4.25 a_0$  and  $4.5 a_0$ . We should stress that this extrapolation is *not* expected to give highly accurate interaction energies for small  $R$ ; we use it simply to define the slope for the cubic spline at  $R = 4.25 a_0$ . The dimer bound state wave functions we compute using our potential energy surface are not sensitive to the highly repulsive small- $R$  region of the potential energy surface.

Beyond  $R = 12.0 a_0$ , we extrapolate each spline using an inverse-power expansion of the form  $\sum_n C_n/R^n$ , including terms with  $n = 5$  and  $6$  in the extrapolations for  $A_{2,2,4}$ , terms with  $n = 6, 8$ , and  $10$  for  $A_{0,0,0}$ , and terms with  $n = 6$  and  $8$  in the extrapolations for  $A_{0,2,2}$  and  $A_{2,0,2}$ . All  $C_n$  coefficients are determined as functions of  $r_1$  and  $r_2$ . The  $C_5$  coefficient for  $A_{2,2,4}$  is computed from the  $\text{H}_2$  quadrupole moments listed in Ref. 47. The  $C_6$  coefficients are obtained from the isotropic and anisotropic  $R^{-6}$  dispersion energy coefficients given in Ref. 48 and the expressions given in Ref. 49. The  $C_8$  and  $C_{10}$  dispersion energy coefficients are obtained from Ref. 50.

To reduce the discontinuities in the higher-order derivatives of the coefficients at  $R = 12.0 a_0$ , where the cubic spline meets the long-range inverse-power extrapolating function, we use the long-range function to compute values of the  $A_{l_1, l_2, L}$  coefficients at six evenly spaced ‘‘phantom’’ points ranging from  $R = 13.0 a_0$  to  $R = 18.0 a_0$ , and force the spline to intercept these phantom points as well as the points computed at the 19  $R$  values cited above. At  $R = 18.0 a_0$ , we also constrain the slope of the spline to match that of the inverse-power expansion. However, we only use the spline to evaluate the coefficients between  $R = 4.25 a_0$  and  $R = 12.0 a_0$ ; beyond  $R = 12.0 a_0$ , we use the inverse-power expansion to compute the

coefficients  $A_{l_1, l_2, L}$ .

Using these extrapolated cubic splines, we can compute the coefficients  $A_{l_1, l_2, L}(R, r_1, r_2)$  at any  $R$  for the discrete pairs of  $\text{H}_2$  bond lengths  $(r_1, r_2)$  at which we performed the ab initio calculations described above. As the last step in defining a smooth potential energy surface, we fit these interpolated (or extrapolated) coefficients to the expression

$$\sum_{k=0}^2 \sum_{n=0}^2 c_{k,n} (r_1 - r_{\text{eq}})^k (r_2 - r_{\text{eq}})^n \quad (7)$$

where  $r_{\text{eq}} = 1.4 a_0$ .

Figure 1 shows how the isotropic coefficient  $A_{0,0,0}(R, r_1, r_2)$ , vibrationally averaged over the ground state vibrational wave functions of the two  $\text{H}_2$  monomers, depends on  $R$  both in the small- $R$ , repulsive region of the potential energy surface and in the shallow  $\text{H}_2$ - $\text{H}_2$  well. We compare the vibrationally-averaged  $A_{0,0,0}$  coefficient computed in this work with a modified ab initio potential energy surface<sup>18</sup> that gives accurate predictions for the low-temperature second virial coefficient of  $\text{H}_2$  gas, with the extrapolated CCSD(T) ab initio calculations of Diep and Johnson,<sup>14,15</sup> and with an empirical isotropic potential energy curve<sup>51</sup> obtained from an analysis of the total scattering cross section of moderate energy  $\text{H}_2$ - $\text{D}_2$  collisions.

In the shallow well, our vibrationally averaged  $A_{0,0,0}$  coefficient agrees fairly well with the extrapolated CCSD(T) results,<sup>14,15</sup> which were computed within the rigid-rotor approximation using the  $v = 0$  vibrationally averaged bond length for both  $\text{H}_2$  monomers. The repulsive wall of our isotropic potential energy curve is slightly softer than that of the extrapolated CCSD(T) curve; our repulsive wall closely tracks the shape of the modified ab initio potential energy surface<sup>18</sup> that gives accurate second virial coefficients, except that our repulsive wall is shifted to slightly larger  $R$  values. It is interesting to note that in the small- $R$  repulsive region, the empirical isotropic potential energy curve<sup>51</sup> derived from scattering data is considerably softer than any of the three curves derived from ab initio computations.

### III. COMPUTATION OF DIMER BOUND STATE ENERGIES

We assess the quality of our potential energy surface by using it to compute the energies of several bound (and long-lived quasibound) states of the  $(\text{H}_2)_2$ ,  $\text{H}_2$ - $\text{D}_2$ , and  $(\text{D}_2)_2$  dimers.

In this section, we summarize the methods used to compute these energies; the energies themselves are presented in later sections. We employ a standard close-coupled approach<sup>30</sup> in which the nine-dimensional dimer wave function is written as

$$\Psi(\mathbf{R}, \mathbf{r}_1, \mathbf{r}_2) = R^{-1} \sum_{\lambda} F_{\lambda}(R) I_{J,M,\gamma}(\hat{\mathbf{R}}, \hat{\mathbf{r}}_1, \hat{\mathbf{r}}_2) \phi_{v_1,j_1}(r_1) \phi_{v_2,j_2}(r_2) . \quad (8)$$

Here  $\mathbf{r}_i$  is the vector separating the two nuclei of  $\text{H}_2$  molecule  $i$ ,  $\mathbf{R}$  is the vector separating the two molecules' centers of mass, and  $\hat{\mathbf{r}}_i$  and  $\hat{\mathbf{R}}$  are the corresponding unit vectors. The quantum numbers  $J$  and  $M$  represent respectively the total angular momentum of the dimer (excluding nuclear spin angular momentum) and its projection on a space-fixed  $z$  axis. The angular basis functions  $I_{J,M,\gamma}$ , which are defined as

$$I_{J,M,\gamma}(\hat{\mathbf{R}}, \hat{\mathbf{r}}_1, \hat{\mathbf{r}}_2) = \sum_{m_1, m_2, M_{12}, N} C(j_1, m_1, j_2, m_2; J_{12}, M_{12}) \\ \times C(J_{12}, M_{12}, L, N; J, M) Y_{j_1, m_1}(\hat{\mathbf{r}}_1) Y_{j_2, m_2}(\hat{\mathbf{r}}_2) Y_{L, N}(\hat{\mathbf{R}}) , \quad (9)$$

couple the rotational angular momenta  $(j_1, j_2)$  of the two  $\text{H}_2$  molecules with the orbital angular momentum  $L$  of the dimer to create functions of definite  $J$  and  $M$ ; we use  $\gamma$  to represent the collection of angular momentum quantum numbers  $(j_1, j_2, J_{12}, L)$ , where  $J_{12}$  is the quantum number corresponding to the (vector) sum of the rotational angular momenta of the two  $\text{H}_2$  molecules. The summation index  $\lambda$  represents a collection of eight quantum numbers: the four quantum numbers listed in  $\gamma$ , the total angular momentum quantum numbers  $J$  and  $M$ , and the vibrational quantum numbers  $v_1$  and  $v_2$  of the two monomers. The functions  $\phi_{v,j}(r)$  are  $\text{H}_2$  monomer radial wave functions, defined so that

$$\int_0^{\infty} \phi_{v,j}^*(r) \phi_{v',j'}(r) dr = \delta_{v,v'} \delta_{j,j'} \quad (10)$$

and obtained from a Numerov–Cooley<sup>52</sup> analysis of the Kolos–Wolniewicz<sup>53</sup>  $\text{H}_2$  potential energy curve.

The dimer radial functions  $F_{\lambda}(R)$  are solutions to a set of coupled second-order differential equations; the  $R$ -dependent terms that couple the radial functions  $F_{\lambda}(R)$  and  $F_{\lambda'}(R)$  are obtained by integrating the six-dimensional  $\text{H}_2$ – $\text{H}_2$  potential energy surface over the eight coordinates  $(\mathbf{r}_1, \mathbf{r}_2, \hat{\mathbf{R}})$ , and are defined by replacing the rigid-rotor potential coefficients  $A_{l_1, l_2, L}(R)$  in Eq. (9) of Ref. 30 with the corresponding vibrationally averaged coefficients

$$\langle v_1, j_1; v_2, j_2 | A_{l_1, l_2, L}(R, r_1, r_2) | v'_1, j'_1; v'_2, j'_2 \rangle = \\ \int_0^{\infty} \int_0^{\infty} \phi_{v_1, j_1}^*(r_1) \phi_{v_2, j_2}^*(r_2) A_{l_1, l_2, L}(R, r_1, r_2) \phi_{v_1, j_1}(r_1) \phi_{v_2, j_2}(r_2) dr_1 dr_2 . \quad (11)$$

We use the ABVN program<sup>54</sup> to evaluate the angular momentum coupling coefficients that appear in Eq. (9) of Ref. 30.

We convert the set of coupled second-order differential equations to a matrix eigenproblem by discretizing the equations on a grid in  $R$ , ranging from  $R_{\min} = 3.0 a_0$  to  $R_{\max} = 28.0 a_0$  in steps of  $0.1 a_0$ , and replacing the dimer radial kinetic energy operator with a five-point central difference approximation evaluated on the grid. (Convergence tests show that using a smaller step size or a larger value of  $R_{\max}$  does not change significantly the energies of the dimer states considered here.) We then solve the matrix eigenproblem using the ARPACK code<sup>55</sup> driven by the SYMMLQ linear algebra routine.<sup>56</sup> We truncate the wave function expansion given in Eq. (8) by limiting  $j_1$  and  $j_2$  to the values 0, 2, and 4, with the additional restriction that  $j_1 + j_2 \leq 6$ , and by limiting  $v_1$  and  $v_2$  to the values 0 and 1. We also assume that the three vibrational manifolds defined by  $v_t = v_1 + v_2 = 0, 1, \text{ or } 2$  are effectively decoupled from one another, which further reduces the size of the matrix eigenproblem. The energies of the  $(v, j)$  rovibrational states of the  $\text{H}_2$  and  $\text{D}_2$  monomers and the dimer reduced masses, which appear in the close-coupled equations for the radial functions  $F_\lambda(R)$ , are computed from the parameters listed in Table III.

Because we consider only even values of  $j_1$  and  $j_2$  here, the parity of the angular basis function  $I_{J,M,\gamma}$  is controlled by the dimer orbital angular momentum quantum number  $L$ ; when  $L$  is even,  $I_{J,M,\gamma}$  has even parity. Angular basis functions with different parities are not coupled together by Eq. (8). In addition, for a dimer of two identical monomers, the overall spatial wave function (exclusive of spin) must be either symmetric or antisymmetric under exchange of the two monomers, and the overall spin wave function must also be symmetric or antisymmetric under monomer exchange. The total wave function, which is the product of the spatial and spin wave functions, must be symmetric or antisymmetric under monomer exchange for bosonic and fermionic monomers, respectively.

The *para*- $\text{H}_2$  molecule is a spin-zero composite boson. For a dimer of such bosons, no exchange-antisymmetric spin wave function can be constructed, and therefore only states whose spatial wave functions are symmetric under monomer exchange are physically admissible. These exchange-symmetric spatial wave functions are the only  $(\text{H}_2)_2$  wave functions considered here. On the other hand, *ortho*- $\text{D}_2$  molecules may have a total nuclear spin quantum number of either zero or two, and it is possible to construct  $(\text{ortho-D}_2)_2$  dimers that have either an exchange-symmetric or an exchange-antisymmetric spin wave function.

Consequently the spatial wave function for (*ortho*-D<sub>2</sub>)<sub>2</sub> may also be either symmetric or antisymmetric under monomer exchange, provided that the total (spin times spatial) (*ortho*-D<sub>2</sub>)<sub>2</sub> wave function is symmetric under monomer exchange.<sup>57</sup>

To check that our matrix-based implementation of the close-coupled formalism is correct, we have used the BOUND code<sup>58</sup> to compute the energies of the (H<sub>2</sub>)<sub>2</sub>, H<sub>2</sub>-D<sub>2</sub>, and (D<sub>2</sub>)<sub>2</sub> bound states that correlate with the monomers' ( $v, j$ ) = (0, 0) ground rovibrational states, and compare these energies with those obtained from our matrix-based code. [Because the BOUND code employs the rigid-rotor approximation, for this comparison we ignore the  $j$  dependence of the monomer radial wave functions  $\phi_{v,j}(r)$  that appear in Eq. (8) and replace these radial wave functions with those for the monomers' ground rovibrational states. This is equivalent to neglecting centrifugal distortion effects on the monomer radial wave functions.] The good agreement between these two calculations confirms the validity of our matrix-based close-coupled approach.

Some of the dimer states discussed below are long-lived quasibound states that can decay via rotational predissociation. The energies reported for these states are those obtained following the “infinite wall” procedure outlined by Grabenstetter and Le Roy,<sup>59</sup> in which the energy of the quasibound state is monitored as  $R_{\max}$  is decreased in 0.1  $a_0$  steps. We estimate that using a finite step size of 0.1  $a_0$  in this procedure introduces an uncertainty in the quasibound state energies of no more than 0.002 cm<sup>-1</sup>.

#### IV. EMPIRICAL ADJUSTMENTS TO THE POTENTIAL ENERGY SURFACE

In this section, we show that if we make two small empirical modifications to our ab initio potential energy surface, it gives rotational and rovibrational transition energies for (H<sub>2</sub>)<sub>2</sub>, H<sub>2</sub>-D<sub>2</sub>, and (D<sub>2</sub>)<sub>2</sub> dimers in good agreement with those obtained experimentally. The two modifications involve a small inward shift of the repulsive wall of the potential energy surface, which we quantify using an adjustable parameter  $s$ , and a slight increase in the magnitude of the surface's  $A_{2,2,4}$  term, which we quantify using an adjustable parameter  $q$ . The unmodified, purely ab initio potential energy surface is defined by  $(s, q) = (0, 0)$ .

We focus first on H<sub>2</sub>-D<sub>2</sub> and (D<sub>2</sub>)<sub>2</sub> dimer states that correlate with rotationally cold ( $j = 0$ ) monomers as  $R \rightarrow \infty$ . Because the wave functions of these states are overwhelmingly dominated by angular basis functions  $I_{J,M,\gamma}$  with  $j_1 = j_2 = 0$  in Eq. (8), the states' energies

are insensitive to the anisotropic terms ( $A_{0,2,2}$ ,  $A_{2,0,2}$ , and  $A_{2,2,4}$ ) of the potential energy surface; however, the states' energies are very sensitive to the location of the surface's repulsive wall. We therefore find the optimal value for  $s$  by adjusting  $s$  to bring the computed energies for transitions involving these states into good agreement with experimentally-measured transition energies.

Next we consider IR-active transitions of the  $\text{H}_2\text{-D}_2$  dimer which involve either (1) a pure vibrational transition  $v = 1 \leftarrow 0$  in the  $\text{H}_2$  monomer and a pure rotational transition  $j = 2 \leftarrow 0$  in the  $\text{D}_2$  monomer, or (2) a rovibrational transition  $(v, j) = (1, 2) \leftarrow (0, 0)$  in the  $\text{H}_2$  monomer and no excitation of the  $\text{D}_2$  monomer. These transitions involve final states whose energies are sensitive to the  $A_{0,2,2}$  and  $A_{2,0,2}$  anisotropic terms of the dimer potential energy surface. We find that, once the repulsive wall of the potential energy surface has been shifted inward slightly, the energies computed for these transitions are in good agreement with experimental measurements. This suggests that the  $A_{0,2,2}$  and  $A_{2,0,2}$  terms of the shifted potential energy surface are accurate, at least in the range of  $R$  values probed by the  $\text{H}_2\text{-D}_2$  dimer wave functions.

Finally, we examine  $(\text{H}_2)_2$  and  $(\text{D}_2)_2$  dimer states which correlate with  $R \rightarrow \infty$  limits involving one  $j = 0$  and one  $j = 2$  molecule. Some of these states have energies that are very sensitive to the strength of the  $A_{2,2,4}$  term of the potential energy surface. By examining how the computed energies for transitions involving these states change with  $q$ , we find the value for  $q$  that gives the best overall agreement with experimental measurements.

### A. Combination differences from the $\text{H}_2\text{-D}_2$ and $(\text{D}_2)_2$ dimer $\text{Q}_1(0)$ infrared spectra

We begin by computing the  $J = 2 \leftarrow 0$  spacings for the  $\text{H}_2\text{-D}_2$  and  $(\text{D}_2)_2$  dimers that correlate with rotationally cold ( $j = 0$ ) monomers; we perform these computations both for the dimers'  $v_t = 0$  ground vibrational manifolds and for the  $v_t = 1$  manifold accessed by IR excitation of the  $\text{H}_2$  monomer in the  $\text{H}_2\text{-D}_2$  dimer. Accurate experimental values for these  $J = 2 \leftarrow 0$  spacings have been obtained from a combination-differences analysis of high-resolution  $\text{H}_2\text{-D}_2$  and  $(\text{D}_2)_2$  IR absorption spectra.<sup>26</sup> Because of the large energy mismatch between the  $v = 1$  levels of  $\text{H}_2$  and  $\text{D}_2$ , in our calculations we assume that the  $\text{H}_2\text{-D}_2$  dimer states correlating with  $\text{H}_2$  ( $v = 1$ ) +  $\text{D}_2$  ( $v = 0$ ) are decoupled from those correlating with  $\text{H}_2$  ( $v = 0$ ) +  $\text{D}_2$  ( $v = 1$ ). (Strictly speaking, the  $v_t = 1$  dimer states accessed in the IR

absorption experiment are quasibound, and can decay through vibrational predissociation. Our assumption that these states are decoupled from the  $v_t = 0$  states, however, closes off this decay channel. Because the lifetimes of the  $v_t = 1$  dimer states are known to be extremely long,<sup>26</sup> this should not materially affect our results.)

Table IV shows that the computed  $J = 2 \leftarrow 0$  spacings are  $0.015 \text{ cm}^{-1}$  to  $0.025 \text{ cm}^{-1}$  lower than the experimental ones. If the dimers were rigid rotors, the  $J = 2 \leftarrow 0$  spacings would be equal to six times the dimers' respective rotational constants. Because the dimers undergo large-amplitude zero-point motion along the  $R$  direction, a rigid-rotor model for the dimers' overall end-over-end rotation is not really appropriate. Nonetheless, this simple-minded picture suggests that the dimer states supported by the computed potential energy surface have average intermolecular distances that are slightly too large, by about  $0.02 a_0$  for the  $(\text{D}_2)_2$  dimer and  $0.03 a_0$  for the  $\text{H}_2\text{-D}_2$  dimer.

As we noted in our discussion of Fig. 1, a small inward shift of the repulsive wall of our potential energy surface would bring it into closer agreement with a surface<sup>18</sup> that gives accurate second virial coefficients for low-temperature  $\text{H}_2$  gas; such a shift would also reduce slightly the average intermolecular distances of the  $\text{H}_2\text{-D}_2$  and  $(\text{D}_2)_2$  dimers, possibly bringing the computed  $J = 2 \leftarrow 0$  spacings into better agreement with experiment. (We note here that the potential energy surface presented in Ref. 18 was itself obtained by a similar inward shift of the repulsive wall of an ab initio computed potential energy surface.) We therefore modify our ab initio  $\text{H}_2\text{-H}_2$  potential energy surface as follows. For  $R$  values below  $6.5 a_0$ , we shift our computed ab initio interaction energies to new, smaller,  $R$  values defined by

$$R_{\text{new}} = R_{\text{old}} - s(6.5 a_0 - R_{\text{old}}) , \quad (12)$$

and then construct a smooth  $s$ -dependent  $\text{H}_2\text{-H}_2$  potential energy surface (as described above in Sec. IID) using the shifted points. Because we have not yet changed the strength of the  $A_{2,2,4}$  term, we are at present implicitly holding  $q$  fixed at  $q = 0$ .

Figure 2 shows how the errors in the  $J = 2 \leftarrow 0$  spacings computed for the  $\text{H}_2\text{-D}_2$  and  $(\text{D}_2)_2$  dimers change as  $s$  increases from  $s = 0$  to  $s = 0.025$ . Choosing  $s = 0.0175$  brings all three of these computed spacings into in excellent agreement with experiment. Fixing  $s$  at this value amounts to an inward shift of the crossing point  $R_0$ , where the vibrationally-averaged  $\text{H}_2\text{-H}_2$  isotropic coefficient  $A_{0,0,0}(R) = 0$ , from  $R_0 = 5.775 a_0$  for the original ab initio potential energy surface (with  $s = 0$ ) to  $R_0 = 5.762 a_0$  for the empirically modified

surface. The corresponding shift for the H<sub>2</sub>-D<sub>2</sub> dimer is from  $R_0 = 5.773 a_0$  to  $R_0 = 5.760 a_0$ ; for the (D<sub>2</sub>)<sub>2</sub> dimer, the shift is from  $R_0 = 5.769 a_0$  to  $R_0 = 5.756 a_0$ .

### B. Q<sub>1</sub>(0) + S<sub>0</sub>(0) and S<sub>1</sub>(0) infrared spectra of the H<sub>2</sub>-D<sub>2</sub> dimer

Next we consider transitions of the H<sub>2</sub>-D<sub>2</sub> dimer in which either (1) the H<sub>2</sub> monomer undergoes a pure  $v = 1 \leftarrow 0$  vibrational transition and the D<sub>2</sub> monomer simultaneously makes a pure  $j = 2 \leftarrow 0$  rotational transition, or (2) the H<sub>2</sub> monomer undergoes the rovibrational transition  $(v, j) = (1, 2) \leftarrow (0, 0)$  while the D<sub>2</sub> monomer remains in its rovibrational ground state. The former transitions belong to the dimer's Q<sub>1</sub>(0) [H<sub>2</sub>] + S<sub>0</sub>(0) [D<sub>2</sub>] band, and the latter transitions to the dimer's S<sub>1</sub>(0) [H<sub>2</sub>] band; for brevity, in this subsection we henceforth drop the molecular labels in square brackets and simply refer either Q<sub>1</sub>(0) + S<sub>0</sub>(0) or S<sub>1</sub>(0) transitions.

Because of the large energy mismatch between the  $j = 2$  states of the H<sub>2</sub> and D<sub>2</sub> molecules, the upper states involved in these transitions are ones in which the  $j = 2$  excitation remains localized on one of the monomers, and thus have energies that are insensitive to the  $A_{2,2,4}$  term of the potential energy surface. The computed energies for these transitions consequently provide insight into the quality of the surface's  $A_{0,0,0}$ ,  $A_{0,2,2}$ , and  $A_{2,0,2}$  terms.

Four relatively sharp Q<sub>1</sub>(0) + S<sub>0</sub>(0) transitions and two relatively sharp S<sub>1</sub>(0) transitions have been observed in the IR absorption spectrum of the H<sub>2</sub>-D<sub>2</sub> dimer.<sup>26</sup> As Table V shows, the potential energy surface with  $s = 0.0175$  gives transition energies for these six transitions in very good agreement with experiment; this suggests that the surface's  $A_{0,2,2}$  and  $A_{2,0,2}$  terms are fairly accurate, at least over the range of  $R$  values for which the H<sub>2</sub>-D<sub>2</sub> dimer has substantial probability density.

### C. S<sub>0</sub>(0) infrared spectra of the (H<sub>2</sub>)<sub>2</sub> and (D<sub>2</sub>)<sub>2</sub> dimers

Finally we consider IR-active transitions of the (H<sub>2</sub>)<sub>2</sub> and (D<sub>2</sub>)<sub>2</sub> dimers that correlate with the S<sub>0</sub>(0)  $j = 2 \leftarrow 0$  pure rotational transitions of the H<sub>2</sub> and D<sub>2</sub> monomers. The upper states involved in these transitions are ones in which the  $j = 2$  excitation is shared by the two monomers; the energies of these states are therefore sensitive to the  $A_{2,2,4}$  term of the dimer potential energy surface, which couples together angular functions in Eq. (8)

with  $(j_1, j_2) = (0, 2)$  and  $(j_1, j_2) = (2, 0)$ .

Because of the low reduced mass of the  $(\text{H}_2)_2$  dimer and the restrictions imposed by nuclear spin statistics, there is just one sharp  $S_0(0)$  IR-active transition for this dimer; it is a  $(J, L) = (1, 1) \leftarrow (0, 0)$  transition and appears in the  $(\text{H}_2)_2$  far-IR absorption spectrum at  $355.425 \text{ cm}^{-1}$ .<sup>28</sup> The transition energy computed for this absorption feature using the  $(s, q) = (0.0175, 0)$  potential energy surface is  $355.438 \text{ cm}^{-1}$ , or  $0.013 \text{ cm}^{-1}$  too high.

The dimer wave function [Eq. (8)] for the upper state of this transition contains significant contributions from only four channels: those with  $(j_1, j_2, J_{12}, L)$  angular momentum quantum numbers of  $(0, 2, 2, 1)$ ,  $(0, 2, 2, 3)$ ,  $(2, 0, 2, 1)$ , and  $(2, 0, 2, 3)$ . Furthermore, only two of these channels give independent contributions to the wave function; for the  $(\text{H}_2)_2$  dimer, exchange symmetry constraints force the channels with  $(j_1, j_2, J_{12}, L) = (a, b, J_{12}, L)$  and  $(j_1, j_2, J_{12}, L) = (b, a, J_{12}, L)$  to, when  $L$  is odd, have radial functions  $F_\lambda(R)$  that are equal in magnitude but opposite in sign. Figure 3 shows the  $F_\lambda(R)$  radial functions for the two independent channels  $(j_1, j_2, J_{12}, L) = (0, 2, 2, 1)$  and  $(0, 2, 2, 3)$  that define the upper state of the  $(J, L) = (1, 1) \leftarrow (0, 0)$  transition; about 97% of the upper state's probability density is associated with the two  $L = 1$  channels.

If we compute the expectation value of the dimer's potential energy using the upper state wave function,

$$\langle V \rangle = \int \int \int |\Psi(\mathbf{R}, \mathbf{r}_1, \mathbf{r}_2)|^2 V(\mathbf{R}, \mathbf{r}_1, \mathbf{r}_2) d\mathbf{R} d\mathbf{r}_1 d\mathbf{r}_2, \quad (13)$$

we find that it includes substantial contributions from the isotropic  $A_{0,0,0}$  term of the potential surface and the anisotropic  $A_{0,2,2}$  and  $A_{2,0,2}$  terms, along with a small contribution from the  $A_{2,2,4}$  term; this last contribution is proportional to the integral

$$\int_0^\infty F_\lambda(R) F_{\lambda'}(R) dR \quad (14)$$

where  $F_\lambda$  and  $F_{\lambda'}$  are the two radial functions shown in Fig. 3. As we explained previously, the lower state for this transition has a wave function dominated by the  $(j_1, j_2) = (0, 0)$  channel, and its potential energy expectation value is therefore sensitive to only the isotropic  $A_{0,0,0}$  term.

This analysis suggests that a small perturbation of the  $A_{2,2,4}$  term will change the energy of the upper state, but not that of the lower state, and could thus bring the computed transition energy for this far-IR absorption feature into better agreement with experiment. Furthermore, because the transitions considered in the preceding two subsections involve

states whose energies are insensitive to  $A_{2,2,4}$ , such a perturbation would preserve the good agreement with experiment observed for those transitions. (Naturally, we could also change the computed transition energy for this particular far-IR absorption feature by adjusting the  $A_{0,2,2}$  and  $A_{2,0,2}$  terms in the potential energy surface; however, such an adjustment would have the undesirable side effect of changing the transition energies computed in the immediately preceding subsection.) Here we adopt a very simple adjustment of the  $A_{2,2,4}$  term, which helps compensate for the fact that the  $A_{2,2,4}$  coefficients computed in Sec. II A include unwanted contributions from the electrostatic QH interaction: we multiply the  $A_{2,2,4}$  coefficients computed at each of the 19  $R$  values by the quantity  $(1 + q)$ , where  $q$  is an adjustable parameter, and then reconstruct the entire potential energy surface as described in Sec. II D.

Figure 4 shows how  $q$  changes the computed position of the  $(\text{H}_2)_2$  dimer's  $(J, L) = (1, 1) \leftarrow (0, 0)$   $S_0(0)$  far-IR absorption feature. At  $q = 0.0235$ , the computed transition energy coincides with the experimental value of  $355.425 \text{ cm}^{-1}$ . (However, the uncertainty of  $\pm 0.005 \text{ cm}^{-1}$  in this experimental transition energy means that a wide range of  $q$  values would be compatible with the experimental observations.) This suggests that a simple rescaling of our  $A_{2,2,4}$  coefficients removes much of the QH interaction's erroneous contribution to these coefficients, even though the QH interaction has a different power-law dependence on  $R$  than does the quadrupole–quadrupole interaction that dominates the  $A_{2,2,4}$  term.

To place tighter constraints on  $q$ , we turn to the  $(\text{D}_2)_2$  dimer, which, because it is both heavier than  $(\text{H}_2)_2$  and has less severe restrictions arising from nuclear spin statistics, exhibits many more absorption features in its far-IR  $S_0(0)$  band.<sup>28</sup> Twelve of these features are relatively sharp, suggesting that they involve bound or long-lived quasibound states, and also have firmly assigned initial- and final-state angular momentum quantum numbers. (We discuss later a thirteenth sharp transition whose initial- and final-state assignments are more tentative.) Figure 5 and Table VI show how the errors in the energies computed for these twelve transitions depend on  $q$ . For the  $q = 0$  potential energy surface, the deviations between computed and measured transition energies range from  $-0.025 \text{ cm}^{-1}$  (transition  $e$ ) to  $+0.064 \text{ cm}^{-1}$  (transition  $h$ ); at  $q = 0.0235$ , however, the computed energies for eight of the twelve transitions (those labeled  $e$  through  $l$ ) agree with experiment to within  $\pm 0.007 \text{ cm}^{-1}$ . Only one of these eight transitions has a computed transition energy that differs from the experimental value by more than  $0.005 \text{ cm}^{-1}$ , which is the experimental uncertainty quoted

for these transitions in Ref. 28. Furthermore, the value  $q = 0.0235$  minimizes the mean absolute deviation between the predicted and observed transition energies for these eight transitions.

The four transitions labeled  $a$  through  $d$  in Table VI exhibit poorer agreement with experiment; furthermore, the errors in the computed energies for these four transitions at  $q = 0.0235$  are equal to or larger in magnitude than the errors at  $q = 0$ . Transition  $c$  corresponds to a very weak far-IR absorption feature; inspection of Fig. 3 in Ref. 28 shows that its intensity is comparable to the level of background noise in the  $(D_2)_2$  absorption spectrum, and it is possible that the true position of this feature differs slightly from that reported in Ref. 28. Transitions  $a$ ,  $b$ , and  $d$ , however, correspond to relatively strong absorption features; furthermore, while transition  $a$  is a shoulder on the low-energy side of a very intense feature (transition  $l$ ), transitions  $b$  and  $d$  are well isolated from other spectral features, and transitions  $a$  and  $b$  are linked by the  $J = 3 \leftarrow 1$  combination difference of the dimer's  $j_1 = j_2 = 0$  manifold. It seems unlikely that the quoted experimental uncertainties for these three transitions could be badly underestimated. It therefore appears that our potential energy surface slightly underpredicts the energies of the  $(J, L) = (2, 2)$  and  $(3, 3)$  excited-state levels accessed via these three IR transitions.

The experimental  $(D_2)_2$   $S_0(0)$  IR absorption spectrum exhibits a thirteenth sharp feature, corresponding to the transition energy  $176.627 \text{ cm}^{-1}$ , which might be either the  $(J, L) = (3, 1) \leftarrow (2, 2)$  transition or the  $(J, L) = (3, 2) \leftarrow (3, 3)$  transition.<sup>28</sup> Our potential energy surface predicts transition energies of  $176.645 \text{ cm}^{-1}$  and  $176.598 \text{ cm}^{-1}$ , respectively, for these transitions.

Finally, we note that the computed transition energies listed in Table V change by only  $0.001$  to  $0.002 \text{ cm}^{-1}$  when the  $(s, q) = (0.0175, 0.0235)$  potential energy surface is used. This validates our decision to hold  $q$  fixed at  $q = 0$  while we find the optimal value for  $s$ , and then hold  $s$  fixed at this value while we find the optimal value for  $q$ .

## V. OTHER COMPARISONS WITH EXPERIMENT

In the previous section, we showed that the quality of the four  $A_{l_1, l_2, L}$  terms of our potential energy surface could be assessed individually by considering transitions between pairs of states that have energies sensitive to specific subsets of these terms. We found that

with two small adjustments to the potential energy surface, we could generate a surface that gives computed transition energies in fairly good agreement with a number of high-resolution experimental measurements.

Although some of the transitions considered in the previous section involve vibrational excitation of the  $\text{H}_2$  monomer in the  $\text{H}_2\text{-D}_2$  dimer, we have not yet considered vibrationally excited states of the  $(\text{H}_2)_2$  or  $(\text{D}_2)_2$  dimers. In these dimers'  $v_t = 1$  vibrationally excited states, the vibrational excitation is delocalized across the pair of monomers; transitions to these excited states therefore probe the simultaneous dependence of the potential energy surface on  $r_1$  and  $r_2$ .

In this section, we show that our modified potential energy surface predicts energies for these transitions that are in good agreement with experiment, indicating that the surface accurately describes the vibrational coupling between the two monomers in the  $(\text{H}_2)_2$  and  $(\text{D}_2)_2$  dimers. We also consider IR-active *double* vibrational transitions of the  $(\text{D}_2)_2$  dimer, in which each monomer undergoes a  $v = 1 \leftarrow 0$  excitation; the good agreement we obtain with experiment provides further evidence that our modified potential energy surface has the correct  $(r_1, r_2)$  dependence.

#### A. $\text{Q}_1(0)$ spectra of the $(\text{H}_2)_2$ , $\text{H}_2\text{-D}_2$ , and $(\text{D}_2)_2$ dimers

Tables VII through IX list the energies of several  $(\text{H}_2)_2$ ,  $\text{H}_2\text{-D}_2$ , and  $(\text{D}_2)_2$  bound states that correlate with  $j = 0$  monomer states, computed using the final  $(s, q) = (0.0175, 0.0235)$  potential energy surface. Using these bound state energies and the monomer  $\text{Q}_1(0)$  transition energies from Table III, we can obtain theoretical positions for the P and R lines in the dimers'  $\text{Q}_1(0)$  IR absorption spectra. In Table X, we list the computed positions for the eleven P and R lines that have been observed experimentally,<sup>26</sup> and compare the computed positions with the observed ones.

The computed transition energies for  $(\text{H}_2)_2$  and  $\text{H}_2\text{-D}_2$  are in excellent agreement with experiment, deviating from the observed energies by amounts smaller than the estimated experimental uncertainties. The transition energies for  $(\text{D}_2)_2$ , however, deviate systematically from the experimental measurements by about  $-0.01 \text{ cm}^{-1}$ , or about twice the estimated uncertainty in the measured transition energies.

To investigate this discrepancy further, we have computed the transition energies of the

$(D_2)_2$  dimer's P(2), P(1), R(0), and R(1) lines using a set of potential energy surfaces with different  $s$  values, keeping  $q$  fixed at  $q = 0.0235$ . (The P and R lines involving  $J = 3$  states have been omitted from this analysis simply because computing these states' energies at several values of  $s$  is very time consuming.) In Fig. 6 we show how the deviations between the computed and observed transition energies change with  $s$ . Only for  $s$  values near 0.0175 do the computed transition energies deviate systematically from experiment; in addition, the  $s = 0.0175$  energies listed in Table IX give  $J = 2 \leftarrow 0$  and  $3 \leftarrow 1$  spacings for both the  $v_t = 0$  and IR-active  $v_t = 1$  manifolds within  $0.002 \text{ cm}^{-1}$  of the experimentally-derived values.<sup>26</sup> These observations suggest that the systematic deviations observed for  $(D_2)_2$  in Table X are not related to a poor choice for  $s$ .

These discrepancies could indicate a small error in the isotropic  $A_{0,0,0}$  term's simultaneous dependence on  $r_1$  and  $r_2$ ; the vibrationally excited  $(D_2)_2$  states involved in the transitions listed in Table X are antisymmetric linear combinations of  $(v_1, v_2) = (0, 1)$  and  $(1, 0)$  states and are therefore sensitive to this  $(r_1, r_2)$  coupling. The same coupling term, however, is also active in the IR-active vibrationally excited  $(H_2)_2$  state, and in the Raman-active  $(H_2)_2$  excited state discussed in the next paragraph, and the agreement with experiment is excellent for transitions involving these states of the  $(H_2)_2$  dimer. More work is needed to understand the systematic deviations in the final column of Table IX.

The  $(H_2)_2$ ,  $H_2\text{-D}_2$ , and  $(D_2)_2$  dimers should all have Raman-active transitions in the vicinity of the monomers'  $Q_1(0)$  Raman transitions; thus far, however, only the  $(H_2)_2$  dimer's Raman spectrum has been observed experimentally.<sup>29</sup> It consists of a single narrow line corresponding to a transition energy of  $4160.78 \pm 0.02 \text{ cm}^{-1}$ . The theoretical  $Q_1(0)$  Raman transition energy for  $(H_2)_2$  derived from the first two lines of Table VII is  $4160.764 \text{ cm}^{-1}$ ; the difference between the computed and experimental Raman transition energies is only slightly smaller than the estimated experimental uncertainty. However, the reported value for the experimental Raman transition energy is based on a value of  $4161.18 \text{ cm}^{-1}$  for the  $Q_1(0)$  transition of an isolated  $H_2$  molecule. The difference between this value and the value used here ( $4161.169 \text{ cm}^{-1}$ ) accounts for more than half the difference between the computed and observed dimer Raman transition energies. If we instead compare the observed and computed dimerization-induced *red shift* of the  $H_2$   $Q_1(0)$  Raman transition, we find that our computed red shift of  $0.405 \text{ cm}^{-1}$  is in excellent agreement with the reported value<sup>29</sup> of  $0.400 \pm 0.02 \text{ cm}^{-1}$ .

### B. $S_1(0)$ and $Q_1(0) + S_1(0)$ infrared spectra of the $(H_2)_2$ and $(D_2)_2$ dimers

We finally use our modified potential energy surface to compute transition energies for features in the  $S_1(0)$  IR absorption bands of the  $(H_2)_2$  and  $(D_2)_2$  dimers, and for features in the  $Q_1(0) + S_1(0)$  IR absorption band of the  $(D_2)_2$  dimer. The  $(D_2)_2$  transitions involve upper states whose energies are sensitive to the  $(r_1, r_2)$  dependence of the potential energy surface.

The  $S_1(0)$  IR absorption spectrum of  $(H_2)_2$  contains just one narrow line,<sup>26</sup> at  $4498.734 \pm 0.004$   $\text{cm}^{-1}$ . This feature is associated with a transition from the dimer's ground state (the first line of Table V) to a state with  $J = L = 1$  that is a linear combination of  $(v_1, j_1; v_2, j_2) = (1, 2; 0, 0)$  and  $(0, 0; 1, 2)$ ; the final state's energy is listed in the first line of Table XI. The  $(s, q) = (0.0175, 0.0235)$  potential energy surface gives a computed  $S_1(0)$  dimer transition energy of  $4498.729$   $\text{cm}^{-1}$ , in excellent agreement with the observed value.

The angular basis functions  $I_{J,M,\gamma}$  in Eq. (8) that correspond to  $(J, L, j_1, j_2) = (1, 1, 0, 2)$  and  $(1, 1, 2, 0)$ , which dominate the final state wave function for this  $S_1(0)$  dimer transition, are not directly coupled together by any of the four terms  $A_{l_1, l_2, L}$  that appear in our potential energy surface; consequently, this  $(H_2)_2$  transition, like the  $H_2$ - $D_2$  transitions considered in Sec. IV B, probes primarily the *monomer* vibrational dependence of the surface's  $A_{0,0,0}$ ,  $A_{0,2,2}$ , and  $A_{2,0,2}$  terms. In contrast to the  $H_2$ - $D_2$  transitions discussed in Sec. IV B, however, the  $(H_2)_2$   $S_1(0)$  transition is sensitive to the  $A_{2,2,0}$  and  $A_{2,2,2}$  terms of the potential energy surface, which we have ignored; the fact that we obtain good agreement with experiment without explicitly including these terms in our surface is further evidence that these terms are of minor importance for the dimer bound states considered in this work.

The  $S_1(0)$  IR absorption band for  $(D_2)_2$  is much richer than that for  $(H_2)_2$ , and is described in Ref. 26 as “possibly [the] most informative of all the hydrogen dimer spectra” presented there. It contains six pairs of narrow lines separated by the  $(D_2)_2$   $v_t = 0$  ground-state  $J = 2 \leftarrow 0$  or  $3 \leftarrow 1$  spacings ( $3.001$   $\text{cm}^{-1}$  and  $4.814$   $\text{cm}^{-1}$ , respectively) and nine additional narrow lines.

The six pairs of lines are associated with transitions from two different rotational levels of the  $v_t = 0$  ground state to a common  $v_t = 1$  upper state level with a firm angular momentum quantum number assignment. The upper part of Table XII compares the computed and experimental transition energies for the higher-frequency transition of each of these pairs.

(No additional information about the quality of our potential energy surface is carried by the other transition of each pair.) The agreement between computed and measured transition energies is quite satisfactory; the largest deviation is  $0.030 \text{ cm}^{-1}$ , for the  $(J, L) = (2, 4) \leftarrow (1, 1)$  transition.

In Ref. 26, initial- and final-state quantum number labels were proposed for the nine other narrow lines that appear in the  $(\text{D}_2)_2$  dimer's  $\text{S}_1(0)$  IR absorption band; these assignments were described as “less certain” than the assignments for the pairs of lines linked by ground-state combination differences. Eight of these lines are listed in the lower part of Table XII, which shows that using these transition assignments, we again observe very good agreement between computed and measured transition energies. (The one line omitted from Table XII involves a transition to a  $J = 4$  state whose energy we have not attempted to compute.) Table XII thus confirms the transition assignments proposed in Ref. 26.

The upper-state wave functions for the transitions listed in Table XII are linear combinations of radial functions in Eq. (8) with angular momentum quantum numbers  $(J, L, j_1, j_2) = (J, L, 0, 2)$  and  $(J, L, 2, 0)$ . For  $L \geq 2$ , these pairs of radial functions are coupled together by the  $A_{2,2,4}$  term of the potential energy surface. In addition, some of the upper states accessed via these transitions are mixtures of  $\text{S}_1(0)$  states, in which the rotational and vibrational excitation reside on the same  $\text{D}_2$  monomer, and  $\text{Q}_1(0) + \text{S}_0(0)$  states, in which one monomer is vibrationally excited while the other is rotationally excited; the quantity  $F$  listed in Table XII measures the degree of mixing in the upper-state wave functions. The good agreement between computed and observed transition energies in Table XII, especially for transitions to upper states with  $L \geq 2$  or with  $F$  values below 0.9, indicates that the  $(r_1, r_2)$  dependence of our potential energy surface, and of the  $A_{2,2,4}$  term in particular, is reasonably accurate.

Further evidence that the  $(r_1, r_2)$  dependence of our potential energy surface is accurate comes from Table XIII, where we compare the computed and observed transition energies for several  $(\text{D}_2)_2$  transitions in the dimer's  $\text{Q}_1(0) + \text{S}_1(0)$  overtone IR absorption band. The agreement between computed and observed transition energies is fairly good, although it appears that the potential energy surface generally underestimates slightly the energies of the upper states of these transitions.

## VI. PREDICTIONS FOR NOT-YET-OBSERVED TRANSITIONS

In this section, we use our final  $(s, q) = (0.0175, 0.0235)$  potential energy surface to predict the energies of some not-yet-observed IR transitions of the  $\text{H}_2\text{-D}_2$  dimer and some not-yet-observed Raman transitions of the  $(\text{H}_2)_2$  and  $(\text{D}_2)_2$  dimers. Experimental studies designed to search for these transitions would help test the accuracy of the potential energy surface presented here.

The region of the  $\text{H}_2\text{-D}_2$  dimer's IR absorption spectrum associated with  $\text{Q}_1(0)$  excitation of the  $\text{H}_2$  monomer has already been studied experimentally, and as Table X shows, our potential energy surface gives accurate transition energies for the four P and R lines in this portion of the dimer's IR spectrum. The dimer should have four additional IR-active P and R lines associated with  $\text{Q}_1(0)$  excitation of the  $\text{D}_2$  monomer. We have computed the transition energies for these four lines based on the dimer binding energies listed in Table VIII; Table XIV lists the predicted transition energies for these four absorption features.

As we noted earlier, the single Raman-active transition in the  $(\text{H}_2)_2$  dimer's  $\text{Q}_1(0)$  band was recently observed. This dimer should also have Raman-active transitions in the monomer  $\text{S}_0(0)$  and  $\text{S}_1(0)$  bands. The energies for these two transitions can be computed from the dimer's ground state binding energy of  $2.894 \text{ cm}^{-1}$  and the binding energies of the  $(J, L) = (2, 0)$  states listed in the second line of Table XI. We therefore predict that the  $(\text{H}_2)_2$  dimer should exhibit  $\text{S}_0(0)$  and  $\text{S}_1(0)$  Raman transitions at  $354.245 \text{ cm}^{-1}$  and  $4497.415 \text{ cm}^{-1}$ , respectively. Unfortunately, these transitions are fairly close to the corresponding Raman-active transitions of the free  $\text{H}_2$  monomer, which are located at transition energies of  $354.373 \text{ cm}^{-1}$  and  $4497.839 \text{ cm}^{-1}$ , so a high-resolution experiment will likely be required to observe the dimer transitions.

Because the  $(\text{D}_2)_2$  dimer has four bound states, its Raman spectrum will be much richer than that of  $(\text{H}_2)_2$ . In Tables XV and XVI we give predictions for Raman-active transitions of the  $(\text{D}_2)_2$  dimer in the monomer  $\text{Q}_1(0)$ ,  $\text{S}_0(0)$ , and  $\text{S}_1(0)$  bands; these predictions are based on the energy levels listed in Tables IX and XVII. There will be additional Raman features in the dimer's  $\text{S}_0(0)$  and  $\text{S}_1(0)$  bands, associated with transitions to final dimer states with  $J = 3$ , which we have omitted from Table XVI because we have not computed the energies of these final dimer states.

## VII. SUMMARY AND DISCUSSION

We have presented a six-dimensional  $\text{H}_2\text{-H}_2$  potential energy surface that accurately describes several bound (and long-lived quasibound) states of the  $(\text{H}_2)_2$ ,  $(\text{D}_2)_2$ , and  $\text{H}_2\text{-D}_2$  dimers that correlate with  $\text{H}_2$  and  $\text{D}_2$  monomers in their  $(v, j) = (0, 0)$ ,  $(0, 2)$ ,  $(1, 0)$ , and  $(1, 2)$  rovibrational states. The surface is based on a set of ab initio  $\text{H}_2\text{-H}_2$  interaction energies that appear to be nearly converged with respect to the one-electron and many-electron basis sets, and which cover fairly densely the region of configuration space associated with the dimer's van der Waals well. The surface incorporates two empirical adjustments: one softens slightly the surface's repulsive wall at small  $\text{H}_2\text{-H}_2$  distances, and one increases slightly the magnitude of the surface's  $A_{2,2,4}$  term that couples the rotational degrees of freedom of the two monomers. The latter adjustment appears to compensate for the fact that our original  $A_{2,2,4}$  coefficients include small contributions from the electrostatic quadrupole-hexadecapole interaction between the two molecules. A Fortran subroutine that evaluates the  $(s, q) = (0.0175, 0.0235)$  potential energy surface is available through EPAPS.<sup>37</sup>

An empirical softening of the ab initio  $\text{H}_2\text{-H}_2$  interaction energy at small intermolecular distances is not unprecedented. For instance, Schaefer and Kohler<sup>18</sup> found that by softening the short-range repulsive wall of an ab initio  $\text{H}_2\text{-H}_2$  potential energy surface, they could bring properties computed using the surface (in this case, the second virial coefficient of  $\text{H}_2$  gas) into better agreement with experiment. The surface of Diep and Johnson<sup>14,15</sup> is based on a series of ab initio calculations that have been extrapolated to the estimated complete one-electron basis set limit; this extrapolation technique yields a surface whose repulsive wall is slightly softer than that of the largest basis-set surface explicitly calculated, and thus has the same effect as an empirical softening of the repulsive wall. It would be interesting to compute the  $\text{H}_2\text{-H}_2$  interaction energy using explicitly-correlated electronic structure methods<sup>60</sup> to see whether lingering basis set incompleteness in the present ab initio calculations is what necessitates the softening of the short-range repulsive wall of the surface.

We have used our potential energy surface to predict the energies of 34 not-yet-observed IR and Raman transitions for  $(\text{H}_2)_2$ ,  $(\text{D}_2)_2$ , and  $\text{H}_2\text{-D}_2$  dimers involving even- $j$  states of the  $\text{H}_2$  and  $\text{D}_2$  monomers. Observations of these transitions could help verify the accuracy of the present potential energy surface, or point out areas where the surface could be further

improved. Calculations of the energy levels of dimers containing one  $j = 1$  molecule, such as *ortho*-H<sub>2</sub>-*para*-H<sub>2</sub>, could also be useful in this regard; these calculations are in progress and will be reported in due course.

### Acknowledgments

Portions of this work were completed while R.J.H. was a sabbatical visitor at the Laboratory for Physical Chemistry in the University of Helsinki Department of Chemistry and a temporary member of the Finnish Center of Excellence in Computational Molecular Science; the hospitality offered by the Laboratory's scientific and administrative staff is greatly appreciated. A. Lignell and M. Metsälä provided valuable advice regarding the use of University of Helsinki computer systems, and a grant of computer time from the Center for Scientific Computing (Espoo, Finland) is gratefully acknowledged. Several conversations with J. M. Fernández (CSIC/IEM, Madrid) were also quite helpful in the final stages of this work. This manuscript was improved considerably by several thoughtful suggestions provided by an anonymous referee, who reviewed it very carefully.

Some of the results reported here were obtained using NWChem version 4.7, as developed and distributed by Pacific Northwest National Laboratory (P. O. Box 999, Richland, WA 99352, USA) and funded by the U. S. Department of Energy.

Financial support was provided by the Air Force Office of Scientific Research through grant F-49620-01-1-0068, by the donors of the Petroleum Research Fund, administered by the American Chemical Society, by the U.S. National Science Foundation through grant CHE-0414705, by a University of Tennessee Professional Development Award, and by a grant from the Suomen Kulttuurirahasto (Finnish Cultural Foundation).

---

\* Electronic address: rhinde@utk.edu

<sup>1</sup> G. Gallup, *Mol. Phys.* **33**, 943 (1977).

<sup>2</sup> P. G. Burton and U. E. Senff, *J. Chem. Phys.* **76**, 6073 (1982).

<sup>3</sup> G. Chałasinski, *Mol. Phys.* **57**, 427 (1986).

<sup>4</sup> P. Hobza, B. Schneider, J. Sauer, P. Carsky, and R. Zahradnik, *Chem. Phys. Lett.* **134**, 418 (1987).

- <sup>5</sup> H. Lavendy, J. M. Robbe, G. Chambaud, and B. Levy, *Chem. Phys.* **116**, 11 (1987).
- <sup>6</sup> B. Schneider, P. Hobza, and R. Zahradnik, *Theo. Chim. Acta*, **73**, 201 (1988).
- <sup>7</sup> U. E. Senff and P. G. Burton, *Aust. J. Phys.* **42**, 47 (1989).
- <sup>8</sup> A. I. Boothroyd, J. E. Dove, W. J. Keogh, P. G. Martin, and M. R. Peterson, *J. Chem. Phys.* **95**, 4331 (1991).
- <sup>9</sup> H. Lavendy, J. M. Robbe, and J. P. Flament, *Chem. Phys. Lett.* **196**, 377 (1992).
- <sup>10</sup> P. Wind and I. Roeggen, *Chem. Phys.* **167**, 247 (1992).
- <sup>11</sup> I. Roeggen and P. Wind, *Chem. Phys.* **167**, 263 (1992).
- <sup>12</sup> P. Wind and I. Roeggen, *Chem. Phys.* **174**, 345 (1993).
- <sup>13</sup> M. Tachikawa, K. Suzuki, K. Iguchi, and T. Miyazaki, *Mol. Simul.* **12**, 291 (1994).
- <sup>14</sup> P. Diep and J. K. Johnson, *J. Chem. Phys.* **112**, 4465 (2000).
- <sup>15</sup> P. Diep and J. K. Johnson, *J. Chem. Phys.* **113**, 3480 (2000).
- <sup>16</sup> C. Kim, S. J. Kim, Y. Lee, and Y. Kim, *Bull. Kor. Chem. Soc.* **21**, 510 (2000).
- <sup>17</sup> A. I. Boothroyd, P. G. Martin, W. J. Keogh, and M. R. Peterson, *J. Chem. Phys.* **116**, 666 (2002).
- <sup>18</sup> J. Schaefer and W. E. Köhler, *Z. Phys. D* **13**, 217 (1989).
- <sup>19</sup> T. H. Dunning, Jr., *J. Chem. Phys.* **90**, 1007 (1989).
- <sup>20</sup> J. Čížek, *J. Chem. Phys.* **45**, 4256 (1966).
- <sup>21</sup> R. J. Bartlett, *J. Phys. Chem.* **93**, 1697 (1989).
- <sup>22</sup> S. K. Pogrebnya and D. C. Clary, *Chem. Phys. Lett.* **363**, 523 (2002).
- <sup>23</sup> B. Maté, F. Thibault, G. Tejeda, J. M. Fernández, and S. Montero, *J. Chem. Phys.* **122**,m 064313 (2005).
- <sup>24</sup> T.-G. Lee, N. Balakrishnan, R. C. Forrey, P. C. Stancil, D. R. Schultz, and G. J. Ferland, *J. Chem. Phys.* **125**, 114302 (2006).
- <sup>25</sup> A. Watanabe and H. L. Welsh, *Phys. Rev. Lett.* **13**, 810 (1964).
- <sup>26</sup> A. R. W. McKellar, *J. Chem. Phys.* **92**, 3261 (1990).
- <sup>27</sup> A. R. W. McKellar, *Faraday Disc.* **97**, 69 (1994).
- <sup>28</sup> A. R. W. McKellar and J. Schaefer, *J. Chem. Phys.* **95**, 3081 (1991).
- <sup>29</sup> G. Tejeda, J. M. Fernández, S. Montero, D. Blume, and J. P. Toennies, *Phys. Rev. Lett.* **92**, 223401 (2004).
- <sup>30</sup> S. Green, *J. Chem. Phys.* **62**, 2271 (1975).

- <sup>31</sup> M. Abramowitz and I. A. Stegun, *Handbook of Mathematical Functions* (National Bureau of Standards: Washington, 1972).
- <sup>32</sup> M. J. Frisch *et al.*, “Gaussian 03, revision B.03”, distributed by Gaussian, Inc. (2003).
- <sup>33</sup> K. Raghavachari, G. W. Trucks, J. A. Pople, and M. Head-Gordon, *Chem. Phys. Lett.* **157**, 479 (1989).
- <sup>34</sup> D. E. Woon and T. H. Dunning, Jr., *J. Chem. Phys.* **100**, 2975 (1994).
- <sup>35</sup> S. F. Boys and F. Bernardi, *Mol. Phys.* **19**, 553 (1970).
- <sup>36</sup> F.-M. Tao and Y.-K. Pan, *J. Chem. Phys.* **97**, 4989 (1992).
- <sup>37</sup> See EPAPS Document No. E-JCPSA6-xxx-xxxxxx for text files containing both the ab initio energies and a Fortran subroutine that computes the H<sub>2</sub>-H<sub>2</sub> potential energy surface. A direct link to this document may be found in the online article’s HTML reference section. The document may also be reached through the EPAPS homepage (<http://www.aip.org/pubservs/epaps.html>) or from <ftp.aip.org> in the directory `/epaps/`. See the EPAPS homepage for more information.
- <sup>38</sup> T. Helgaker *et al.*, DALTON, a molecular electronic structure program, Release 1.2.1, available from (<http://www.kjemi.uio.no/software/dalton/dalton.html>) (2001).
- <sup>39</sup> R. J. Hinde, *Few-Body Syst.* **38**, 187 (2006).
- <sup>40</sup> T. van Mourik and T. H. Dunning, Jr., *J. Chem. Phys.* **111**, 9248 (1999).
- <sup>41</sup> R. J. Hinde, *J. Phys. B: At. Mol. Opt. Phys.* **36**, 3119 (2003).
- <sup>42</sup> J. Noga and R. J. Bartlett, *J. Chem. Phys.* **86**, 7041 (1987).
- <sup>43</sup> J. Noga and R. J. Bartlett, *J. Chem. Phys.* **89**, 3401 (1988).
- <sup>44</sup> S. Hirata, *J. Phys. Chem. A* **107**, 9887 (2003).
- <sup>45</sup> E. Aprà *et al.*, “NWChem: A computational chemistry package for parallel computers, version 4.7”, distributed by the U. S. Department of Energy’s Pacific Northwest National Laboratory, and available from (<http://www.emsl.pnl.gov/docs/nwchem/nwchem.html>) (2005).
- <sup>46</sup> R. A. Kendall, E. Aprà, D. E. Bernholdt, E. J. Bylaska, M. Dupuis, G. I. Fann, R. J. Harrison, J. Ju, J. A. Nichols, J. Nieplocha, T. P. Straatsma, T. L. Windus, and A. T. Wong, *Comput. Phys. Commun.* **128**, 260 (2000).
- <sup>47</sup> L. Wolniewicz, I. Simbotin, and A. Dalgarno, *Astrophys. J. Supp. Series* **115**, 293 (1998).
- <sup>48</sup> R. J. Hinde, *J. Chem. Phys.* **122**, 144304 (2005).
- <sup>49</sup> A. J. Stone and R. J. A. Tough, *Chem. Phys. Lett.* **110**, 123 (1984).
- <sup>50</sup> T. C. Lillestolen and R. J. Hinde, unpublished.

- <sup>51</sup> M. J. Norman, R. O. Watts, and U. Buck, *J. Chem. Phys.* **81**, 3500 (1984).
- <sup>52</sup> J. W. Cooley, *Math. Comput.* **15**, 363 (1961).
- <sup>53</sup> W. Kołos and L. Wolniewicz, *J. Chem. Phys.* **43**, 2429 (1965).
- <sup>54</sup> A. J. Stone and C. P. Woods, *Comput. Phys. Commun.* **21**, 195 (1980).
- <sup>55</sup> R. B. Lehoucq, D. C. Sorensen, and C. Yang, *ARPACK Users' Guide: Solution of Large-Scale Eigenvalue Problems with Implicitly Restarted Arnoldi Methods*, (SIAM: Philadelphia, 1998).  
The ARPACK code is available from <http://www.caam.rice.edu/software/ARPACK>.
- <sup>56</sup> C. C. Paige and M. A. Saunders, *SIAM J. Numer. Anal.* **12**, 617 (1975).
- <sup>57</sup> G. Danby, *J. Phys. B: At. Mol. Opt. Phys.* **22**, 1785 (1989).
- <sup>58</sup> J. M. Hutson, "BOUND computer code, version 5", distributed by Collaborative Computational Project 6 of the UK Science and Engineering Research Council, and available from <http://www.ccp6.ac.uk/downloads.htm> (1994).
- <sup>59</sup> J. E. Grabenstetter and R. J. Le Roy, *Chem. Phys.* **42**, 41 (1979).
- <sup>60</sup> W. Klopper, F. R. Manby, S. Ten-No, E. F. Valeev, *Int. Rev. Phys. Chem.* **25**, 427 (2006).

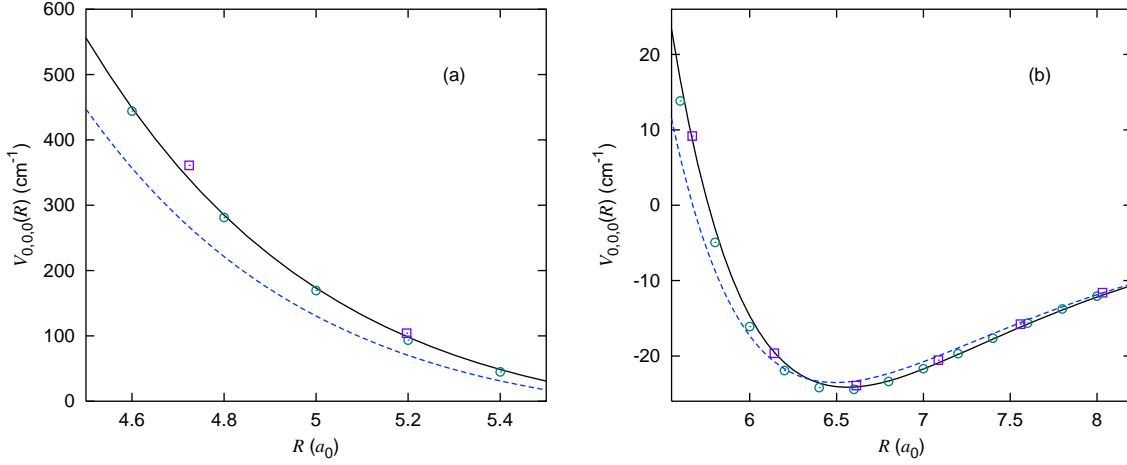


FIG. 1: (Color online.) Comparison of the vibrationally-averaged isotropic  $\text{H}_2\text{-H}_2$  potential energy curve  $A_{0,0,0}(R)$  obtained in this work (solid line) with the isotropic rigid-rotor potential energy curves obtained by other researchers. Boxes represent the extrapolated CCSD(T) potential energy surface of Refs. 14 and 15; circles represent the adjusted ab initio potential of Ref. 18; the dashed line represents the empirical potential of Ref. 51. The solid line shown here is computed from the unmodified  $(s, q) = (0, 0)$  potential energy surface. Panel (a) shows the repulsive wall at small  $R$  values; panel (b) shows the van der Waals well.

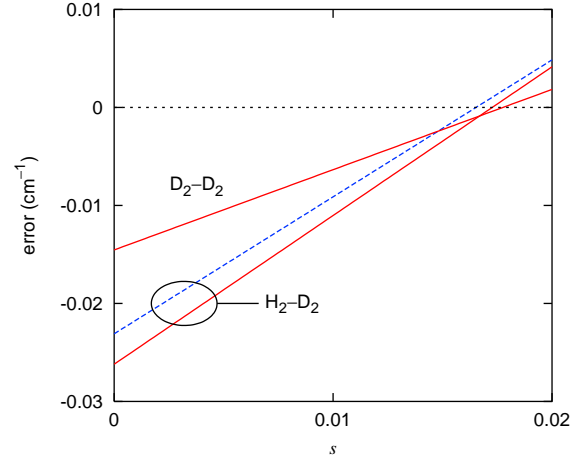


FIG. 2: (Color online.) Dependence on  $s$  of the errors (computed minus experiment) in the  $J = 2 \leftarrow 0$  spacings of the  $\text{H}_2\text{-D}_2$  and  $(\text{D}_2)_2$  dimers. Solid lines are for the vibrationally cold ( $v_t = 0$ ) dimers; the dashed line is for the  $\text{H}_2$  ( $v = 1$ ) +  $\text{D}_2$  ( $v = 0$ ) dimer. The parameter  $q$  is held fixed at  $q = 0$ .

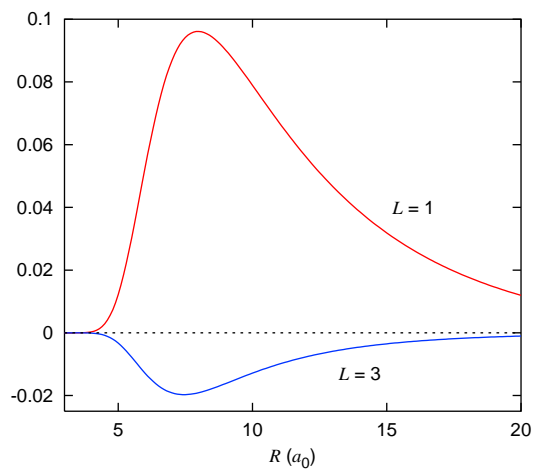


FIG. 3: (Color online). The two dominant  $F_\lambda(R)$  radial functions for the  $(J, L) = (1, 1)$  upper state accessed in the  $(\text{H}_2)_2$  dimer's  $S_0(0)$  IR transition. These functions are computed using the  $(s, q) = (0.0175, 0)$  potential energy surface.

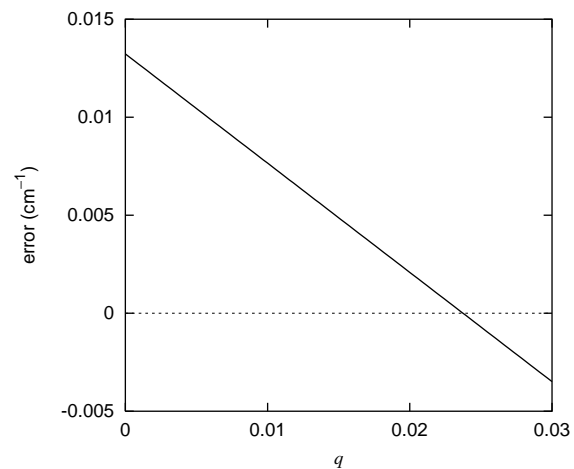


FIG. 4: Dependence on  $q$  of the error (computed minus experiment) in the transition energy computed for the  $(\text{H}_2)_2$  dimer's far-IR  $S_0(0)$  absorption feature. The parameter  $s$  is held fixed at  $s = 0.0175$ .

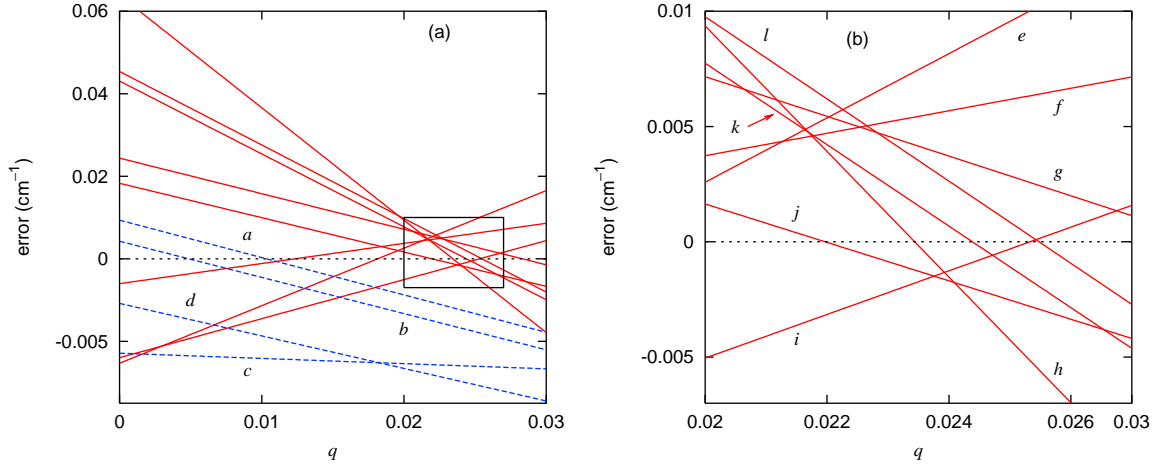


FIG. 5: (Color online.) Dependence on  $q$  of the errors (computed minus experiment) in the transition energies computed for twelve features in the  $(D_2)_2$  dimer's far-IR  $S_0(0)$  absorption band. Panel (b) is a magnification of the small box in panel (a). The labels affixed to each line refer to Table VI. The parameter  $s$  is held fixed at  $s = 0.0175$ .

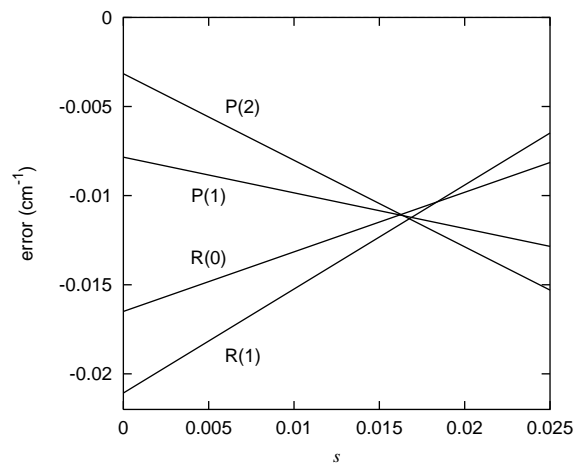


FIG. 6: Dependence on  $s$  of the errors (computed minus experiment) in the transition energies computed for four lines in the  $(D_2)_2$  dimer's  $Q_1(0)$  IR absorption band. The parameter  $q$  is held fixed at  $q = 0.0235$ .

TABLE I: Comparison of angular expansion coefficients  $A_{l_1, l_2, L}$  (in  $\text{cm}^{-1}$ ) computed using two spherical quadrature rules at  $(R, r_1, r_2) = (4.5 a_0, 1.4 a_0, 1.7 a_0)$ . These coefficients do not include the full-triples correction.

$(l_1, l_2, L)$	18-point	24-point
(0, 0, 0)	674.559	674.629
(0, 2, 2)	32.984	33.577
(2, 0, 2)	20.195	20.465
(2, 2, 4)	19.017	19.174
(2, 2, 0)	-0.599	1.413
(2, 2, 2)	0.465	-0.292

TABLE II: Angular expansion coefficients  $A_{l_1, l_2, L}(R, r_1, r_2)$ , in  $\text{cm}^{-1}$ , computed from aug-cc-pVTZ and aug-cc-pVQZ ab initio energies. A (3s3p2d) set of bond functions is used in all calculations. The coefficients are grouped into pairs of rows corresponding to fixed  $(R, r_1, r_2)$ ; the upper row in each pair lists the aug-cc-pVQZ coefficients, while the lower row in each pair lists the aug-cc-pVTZ coefficients. These coefficients do not include the full-triples correction.

$R$ ( $a_0$ )	$(r_1, r_2)$ ( $a_0$ )	$A_{0,0,0}$	$A_{2,0,2}$	$A_{0,2,2}$	$A_{2,2,4}$
4.5	(1.1, 1.1)	378.145	10.026	10.026	6.360
		382.457	10.094	10.094	6.320
4.5	(1.4, 1.4)	570.418	19.989	19.989	14.277
		576.072	20.116	20.116	14.197
4.5	(1.7, 1.7)	776.340	31.141	31.141	24.607
		783.772	31.379	31.379	24.478
4.5	(1.1, 1.7)	573.576	11.959	33.199	13.032
		579.204	11.878	33.480	13.044
5.0	(1.1, 1.1)	101.523	3.023	3.023	3.607
		103.343	3.046	3.046	3.585
5.0	(1.4, 1.4)	174.837	6.794	6.794	8.119
		177.554	6.879	6.879	8.070
5.0	(1.7, 1.7)	262.487	11.883	11.883	14.347
		266.336	12.043	12.043	14.254
5.0	(1.1, 1.7)	178.370	3.853	12.040	7.370
		181.142	3.883	12.179	7.325
6.5	(1.4, 1.4)	-22.530	-0.543	-0.543	2.070
		-22.239	-0.528	-0.528	2.054

TABLE III: Monomer spectroscopic constants (in  $\text{cm}^{-1}$ ) and total masses employed in the dimer bound state calculations.

Species	$\Delta E (v = 1 \leftarrow 0)$	$B (v = 0)$	$B (v = 1)$	Mass ( $m_e$ )
H <sub>2</sub>	4161.169	59.0622	56.1117	3674.3
D <sub>2</sub>	2993.614	29.8445	28.7908	7342.9

TABLE IV: Observed and computed spacings (in  $\text{cm}^{-1}$ ) between the  $J = 0$  and  $J = 2$  states of H<sub>2</sub>-D<sub>2</sub> and D<sub>2</sub>-D<sub>2</sub> dimers that correlate with  $j = 0$  states of the constituent monomers. These bound state computations employ the unmodified  $(s, q) = (0, 0)$  potential energy surface.

Dimer	Observed	Computed
H <sub>2</sub> ( $v = 0$ ) + D <sub>2</sub> ( $v = 0$ )	3.848	3.822
H <sub>2</sub> ( $v = 1$ ) + D <sub>2</sub> ( $v = 0$ )	3.889	3.866
D <sub>2</sub> ( $v = 0$ ) + D <sub>2</sub> ( $v = 0$ )	3.001	2.986

TABLE V: Observed transition energies and deviations between observed and computed transition energies (computed minus experiment), in  $\text{cm}^{-1}$ , for selected IR-active transitions of the H<sub>2</sub>-D<sub>2</sub> dimer involving  $v = 1 \leftarrow 0$  excitation of the H<sub>2</sub> monomer. The D<sub>2</sub> monomer remains in its  $v = 0$  vibrational level during the transition. The initial and final states are identified by the angular momentum quantum numbers associated with the dominant term in the dimer wave function [Eq. (8)];  $j_1$  and  $j_2$  are the angular momenta of the H<sub>2</sub> and D<sub>2</sub> molecules, respectively. The computed transition energies are obtained using the  $(s, q) = (0.0175, 0)$  potential energy surface.

$(J, L, j_1, j_2)' \leftarrow (J, L, j_1, j_2)''$	Observed	Deviation
(1, 1, 0, 2) $\leftarrow$ (2, 2, 0, 0)	4337.046	+0.003
(2, 1, 0, 2) $\leftarrow$ (2, 2, 0, 0)	4337.609	+0.002
(0, 2, 0, 2) $\leftarrow$ (1, 1, 0, 0)	4342.004	+0.013
(1, 2, 0, 2) $\leftarrow$ (1, 1, 0, 0)	4342.208	+0.007
(1, 1, 2, 0) $\leftarrow$ (2, 2, 0, 0)	4494.719	-0.007
(2, 1, 2, 0) $\leftarrow$ (2, 2, 0, 0)	4495.20	+0.009

TABLE VI: Observed transition energies and deviations between observed and computed transition energies (computed minus experiment), in  $\text{cm}^{-1}$ , for IR-active  $(\text{D}_2)_2$  transitions in the  $\text{D}_2 \text{S}_0(0)$  band. The computed transition energies are obtained using either the  $(s, q) = (0.0175, 0)$  or the  $(s, q) = (0.0175, 0.0235)$  potential energy surface.

Label	$(J, L)' \leftarrow (J, L)''$	Observed	Deviation	
			$q = 0$	$q = 0.0235$
<i>a</i>	$(2, 2) \leftarrow (3, 3)$	175.507	+0.010	-0.012
<i>b</i>	$(2, 2) \leftarrow (1, 1)$	180.322	+0.005	-0.016
<i>c</i>	$(2, 1) \leftarrow (2, 2)$	177.359	-0.022	-0.026
<i>d</i>	$(3, 3) \leftarrow (2, 2)$	181.287	-0.010	-0.029
<i>e</i>	$(1, 2) \leftarrow (1, 1)$	182.328	-0.025	+0.007
<i>f</i>	$(1, 3) \leftarrow (0, 0)$	184.536	-0.006	+0.005
<i>g</i>	$(2, 0) \leftarrow (3, 3)$	172.776	+0.024	+0.004
<i>h</i>	$(0, 2) \leftarrow (1, 1)$	177.996	+0.064	+0.000
<i>i</i>	$(2, 3) \leftarrow (2, 2)$	182.797	-0.024	-0.002
<i>j</i>	$(2, 0) \leftarrow (1, 1)$	177.592	+0.018	-0.001
<i>k</i>	$(1, 1) \leftarrow (0, 0)$	178.747	+0.043	+0.002
<i>l</i>	$(1, 1) \leftarrow (2, 2)$	175.744	+0.045	+0.004

TABLE VII: Binding energies (in  $\text{cm}^{-1}$ ) of selected  $(\text{H}_2)_2$  dimer states that correlate with  $j = 0$  states of the constituent monomers. These bound state computations employ the  $(s, q) = (0.0175, 0.0235)$  potential energy surface.

$v_t$	$J$	Binding energy
0	0	2.894
1	0	3.299
1	1	1.554

TABLE VIII: Binding energies (in  $\text{cm}^{-1}$ ) of selected  $\text{H}_2\text{-D}_2$  dimer states that correlate with  $j = 0$  states of the constituent monomers. These bound state computations employ the  $(s, q) = (0.0175, 0.0235)$  potential energy surface.

$J$	Vibrational state		
	$v_t = 0$	$v = 1 (\text{H}_2)$	$v = 1 (\text{D}_2)$
0	4.417	4.792	4.644
1	3.074	3.442	3.299
2	0.568	0.902	0.775

TABLE IX: Binding energies (in  $\text{cm}^{-1}$ ) of selected  $(\text{D}_2)_2$  dimer states that correlate with  $j = 0$  states of the constituent monomers. The letters S and A indicate that the state is respectively symmetric or antisymmetric under monomer exchange. These bound state computations employ the  $(s, q) = (0.0175, 0.0235)$  potential energy surface.

$J$	Vibrational state		
	$v_t = 0$	$v_t = 1 (\text{S})$	$v_t = 1 (\text{A})$
0	6.712 (S)	7.118	6.939
1	5.696 (A)	5.925	6.101
2	3.711 (S)	4.111	3.941
3	0.885 (A)	1.109	1.263

TABLE X: Computed transition energies (in  $\text{cm}^{-1}$ ) and deviations from experiment (computed minus experiment) of the P and R lines in the  $Q_1(0)$  IR bands of the  $(\text{H}_2)_2$ ,  $\text{H}_2\text{-D}_2$ , and  $(\text{D}_2)_2$  dimers. For the  $\text{H}_2\text{-D}_2$  dimer, the vibrationally excited state correlates with  $v = 1 \text{ H}_2 + v = 0 \text{ D}_2$ ; for the  $(\text{H}_2)_2$  and  $(\text{D}_2)_2$  dimers, the vibrational excitation is delocalized antisymmetrically across the two monomers. The computed transition energies are obtained using the  $(s, q) = (0.0175, 0.0235)$  potential energy surface.

$J' \leftarrow J''$	$(\text{H}_2)_2$		$\text{H}_2\text{-D}_2$		$(\text{D}_2)_2$	
	Computed	Deviation	Computed	Deviation	Computed	Deviation
$2 \leftarrow 3$	—	—	—	—	2990.558	-0.007
$1 \leftarrow 2$	—	—	4158.296	-0.003	2991.400	-0.012
$0 \leftarrow 1$	—	—	4159.451	-0.001	2992.371	-0.011
$1 \leftarrow 0$	4162.509	-0.004	4162.144	-0.003	2994.401	-0.011
$2 \leftarrow 1$	—	—	4163.341	+0.000	2995.368	-0.011
$3 \leftarrow 2$	—	—	—	—	2996.216	-0.013

TABLE XI: Energies (in  $\text{cm}^{-1}$ ) for  $(\text{H}_2)_2$  states with  $J_{12} = 2$ ,  $v_t = 0$  or 1, and  $L \leq 1$ . The energies are obtained using the  $(s, q) = (0.0175, 0.0235)$  potential energy surface, and are given relative to the  $S_0(0)$  and  $S_1(0)$   $\text{H}_2$  monomer energies for  $v_t = 0$  and 1, respectively.

$(J, L)$	Energy	
	$v_t = 0$	$v_t = 1$
(1, 1)	-1.842	-2.004
(2, 0)	-3.022	-3.318
(2, 1)	-1.191	-1.463

TABLE XII: Observed transition energies and deviations between observed and computed transition energies (computed minus experiment), in  $\text{cm}^{-1}$ , for IR-active  $(D_2)_2$  transitions in the  $D_2$   $S_1(0)$  band. The computed transition energies are obtained using the  $(s, q) = (0.0175, 0.0235)$  potential energy surface. The column labeled  $F$  indicates the fraction of upper-state probability associated with functions in Eq. (8) in which the  $v = 1$  and  $j = 2$  molecular excitations reside on the same monomer.

$(J, L)' \leftarrow (J, L)''$	Observed	Deviation	$F$
$(2, 0) \leftarrow (1, 1)$	3164.705	-0.005	0.984
$(1, 1) \leftarrow (0, 0)$	3166.195	-0.005	0.959
$(2, 2) \leftarrow (1, 1)$	3167.890	-0.004	0.966
$(1, 3) \leftarrow (0, 0)$	3169.919	-0.020	0.666
$(2, 0) \leftarrow (1, 1)$	3170.429	-0.020	0.196
$(2, 4) \leftarrow (1, 1)$	3173.702	+0.030	0.467
$(3, 2) \leftarrow (3, 3)$	3163.378	-0.009	0.993
$(3, 1) \leftarrow (2, 2)$	3163.707	-0.003	0.989
$(2, 1) \leftarrow (2, 2)$	3164.281	-0.011	0.992
$(0, 2) \leftarrow (1, 1)$	3166.340	-0.004	0.871
$(1, 2) \leftarrow (1, 1)$	3167.392	-0.030	0.942
$(2, 3) \leftarrow (2, 2)$	3168.343	-0.028	0.860
$(3, 3) \leftarrow (2, 2)$	3168.737	-0.004	0.891
$(2, 1) \leftarrow (2, 2)$	3170.931	+0.003	0.298

TABLE XIII: Observed transition energies and deviations between observed and computed transition energies (computed minus experiment), in  $\text{cm}^{-1}$ , for IR-active  $(D_2)_2$  transitions in the  $D_2 Q_1(0) + S_1(0)$  band. The computed transition energies are obtained using the  $(s, q) = (0.0175, 0.0235)$  potential energy surface.

$(J, L)' \leftarrow (J, L)''$	Observed	Deviation
$(2, 0) \leftarrow (3, 3)$	6152.870	-0.018
$(1, 1) \leftarrow (2, 2)$	6155.672	-0.020
$(2, 2) \leftarrow (3, 3)$	6155.672	-0.021
$(3, 1) \leftarrow (2, 2)$	6156.767	-0.015
$(0, 2) \leftarrow (1, 1)$	6157.770	-0.003
$(1, 1) \leftarrow (0, 0)$	6158.669	-0.016
$(3, 3) \leftarrow (2, 2)$	6161.471	-0.036
$(1, 2) \leftarrow (1, 1)$	6162.773	-0.002
$(2, 3) \leftarrow (2, 2)$	6163.261	-0.015
$(1, 3) \leftarrow (0, 0)$	6164.872	-0.005

TABLE XIV: Predicted transition energies (in  $\text{cm}^{-1}$ ) of the P and R lines in the  $Q_1(0)$  IR band of the  $H_2-D_2$  dimer, for vibrationally excited states correlating with  $v = 0 H_2 + v = 1 D_2$ . The predictions are obtained using the  $(s, q) = (0.0175, 0.0235)$  potential energy surface.

$J' \leftarrow J''$	Energy
$1 \leftarrow 2$	2990.884
$0 \leftarrow 1$	2992.044
$1 \leftarrow 0$	2994.732
$2 \leftarrow 1$	2995.913

TABLE XV: Predicted transition energies (in  $\text{cm}^{-1}$ ) for Raman-active transitions in the  $Q_1(0)$  band of the  $(D_2)_2$  dimer. The predictions are obtained using the  $(s, q) = (0.0175, 0.0235)$  potential energy surface.

$(J, L)' \leftarrow (J, L)''$	Energy
$(1, 1) \leftarrow (3, 3)$	2988.398
$(0, 0) \leftarrow (2, 2)$	2990.207
$(0, 0) \leftarrow (0, 0)$	2993.208
$(1, 1) \leftarrow (1, 1)$	2993.209
$(2, 2) \leftarrow (2, 2)$	2993.214
$(3, 3) \leftarrow (3, 3)$	2993.236
$(2, 2) \leftarrow (0, 0)$	2996.215
$(3, 3) \leftarrow (1, 1)$	2998.047

TABLE XVI: Predicted transition energies (in  $\text{cm}^{-1}$ ) for Raman-active transitions in the  $S_0(0)$  and  $S_1(0)$  bands of the  $(D_2)_2$  dimer. The predictions are obtained using the  $(s, q) = (0.0175, 0.0235)$  potential energy surface.

$(J, L)' \leftarrow (J, L)''$	$S_0(0)$ energy	$S_1(0)$ energy
$(0, 2) \leftarrow (0, 0)$	183.837	3167.595
$(2, 0) \leftarrow (0, 0)$	178.713	3165.725
$(2, 2) \leftarrow (0, 0)$	182.694	3168.981
$(1, 1) \leftarrow (1, 1)$	178.108	3165.208
$(1, 3) \leftarrow (1, 1)$	184.568	3168.916
$(0, 2) \leftarrow (2, 2)$	180.836	3164.594
$(2, 0) \leftarrow (2, 2)$	175.712	3162.724
$(2, 2) \leftarrow (2, 2)$	179.693	3165.980
$(1, 1) \leftarrow (3, 3)$	173.298	3160.397
$(1, 3) \leftarrow (3, 3)$	179.758	3164.105

TABLE XVII: Energies (in  $\text{cm}^{-1}$ ) for  $(\text{D}_2)_2$  states with  $J_{12} = 2$ ,  $v_t = 0$  or 1, and  $J \leq 2$ . The energies are obtained using the  $(s, q) = (0.0175, 0.0235)$  potential energy surface, and are given relative to the  $S_0(0)$  and  $S_1(0)$   $\text{D}_2$  monomer energies for  $v_t = 0$  and 1, respectively.

$(J, L)$	Exchange	Energy	Energy
	symmetry	$v_t = 0$	$v_t = 1$
(0, 2)	S	-1.942	-5.476
(1, 1)	S	-7.030	-6.881
(1, 2)	S	-5.620	-4.850
(1, 3)	S	-1.238	-3.172
(2, 0)	S	-7.066	-7.347
(2, 1)	S	-5.445	-5.800
(2, 2)	S	-3.085	-4.090
(2, 3)	S	+0.017	-1.754
(0, 2)	A	-6.767	-5.719
(1, 1)	A	-6.654	-6.846
(1, 2)	A	-2.427	-4.692
(1, 3)	A	-0.194	-3.138
(2, 0)	A	-7.172	-7.356
(2, 1)	A	-5.752	-5.821
(2, 2)	A	-4.457	-4.169
(2, 3)	A	-1.813	-1.844